Supporting Information

Converting Waste PET into Dimethyl Terephthalate and Diverse Boronic Esters under Metal-free Conditions

Minghao Zhang,[a] Yunkai Yu,[a] Zhuo Wang,[a] Shaoyu Zhang,[a] Xiong Gao,[a] Jiaming Liu,[a] Jing Li,[de] Weixiang Wu[abc], Qingqing Mei[abc*]

[a]Institute of Environment Science and Technology, College of Environmental and Resource Sciences, Zhejiang University, Hangzhou 310058, Zhejiang, China.

[b]Key Laboratory of Environment Remediation and Ecological Health, Ministry of Education, College of Environmental Resource Sciences, Zhejiang University, 310058 Hangzhou, China.

[c]Zhejiang Province Key Laboratory for Water Pollution Control and Environmental Safety Technology, Zhejiang 310058, China.

[d]Key Laboratory of Biomass Chemical Engineering of Ministry of Education, College of Chemical and Biological Engineering, Zhejiang University, Hangzhou, 310058, Zhejiang, China.

[e]Institute of Zhejiang University-Quzhou, 99 Zheda Road, Quzhou, 324000, Zhejiang, China.

*Corresponding author: Qingqing Mei

Address: 866 Yuhangtang Road, Hangzhou 310058, China.

E-mail address: meiqq@zju.edu.cn

Table of Contents

1. Experimental

1.1. Materials

Analytical grade solvents and commercially available reagents were purchased from commercial sources and used directly without further purification unless otherwise stated. PET Powder (0.075 mm, Made from Bottle-grade PET Chip, CR Chem-MAT CR-8863), poly(ethylene glycol succinate) (98%, Bide Pharmatech Ltd.), poly(ethylene adipate) (Mw: ~1000, Aladdin), poly(ethylene 2,5-furandicarboxylate) (Alfa) and poly(propylene carbonate) (Mn: ~5000, Rhawn), 4-tolylboronic acid (>99%, Leyan), phenylboronic acid (97%, Meryer), (4-isopropylphenyl)boronic acid (98%, Shanghai D&B), (4-(*tert*-butyl)phenyl)boronic acid (97%, Heowns), 4-methoxybenzeneboronic acid (98%, Macklin), (4-hydroxyphenyl)boronic acid (98%, Shanghai D&B), (4-fluorophenyl)boronic acid (98%, Shanghai D&B), (4-chlorophenyl)boronic acid (98%, Shanghai D&B), (4-bromophenyl)boronic acid (98%, Shanghai D&B), (4-(methoxycarbonyl)phenyl)boronic acid (97%, Meryer), (4-(trifluoromethyl)phenyl)boronic acid (98%, Heowns), (4-acetylphenyl)boronic acid (98%, Damas-beta), (4-nitrophenyl)boronic acid (99%, Bidepharm), *m*-tolylboronic acid (98%, Meryer), (3-methoxyphenyl)boronic acid (98%, Shanghai D&B), (3-fluorophenyl)boronic acid (97%, Meryer), naphthalen-1-ylboronic acid (98%, Meryer), naphthalen-2-ylboronic acid (99%, Bidepharm), phenanthren-9-ylboronic acid (99%, Bidepharm), thiophen-3-ylboronic acid (98%, Shanghai D&B), (4-(diphenylamino)phenyl)boronic acid (98%, Shanghai D&B), cyclohexylboronic acid (97%, Leyan), 1,4-phenylenediboronic acid (98%, Shanghai D&B), hypodiboric acid (98%, Meryer), 2,4,6-triphenyl-1,3,5,2,4,6-trioxatriborinane (98%, Meryer), 2,4,6-tris(4-fluorophenyl)-1,3,5,2,4,6-trioxatriborinane (98%, Innochem). [EMIm][Cl] (97%, Aladdin), [EMIm][OAc] (98%, Meryer), [EMIm][Br] (98%, Meryer), [EMIm][I] (97%, Rhawn), [EMIm][$MeSO_3$] (98%, Meryer), [EMIm][BF_4] (98%, Meryer), [BMIm][OAc] (98%, Meryer), ethylene glycol (AR, Sinopharm), dichloromethane (AR, Shanghai Linfeng Chemical Reagent CO. LTD), MeOH (>99%, J&K Scientific), $CDCl_3$ (99%, Sigma-Aldrich), DMSO-d_6 (99%, Adamas), and deionized water were used herein.

1.2. Experimental procedures

In-situ EG capturing process

PET powder (1 mmol), [EMIm][OAc] (5% mol), and MeOH (3 mL) were combined in a polytetrafluoroethylene rotor (25 mL), which was then hermetically sealed within a stainless-steel reactor (C-MAG HS 7C S025 (IKA, Germany, 220~230V, 50/60 Hz, 1020 W)). The reactor was stirred at 180°C for 1.5 hours with a rotational speed of 500 r/min on the heating plate. Following the completion of the reaction, the system was quenched by transferring the reactor into an ice bath. Subsequently, the resulting reaction solution was diluted with 10 mL of dichloromethane. The liquid products were subjected to analysis via gas

chromatography (GC), using mesitylene (0.5 mmol) as an internal standard. The yields of PTDB and dimethyl terephthalate (DMT) were calculated using the following equation:

$$PTDB\ Yield\ (\%) = \frac{PTDB\ \ amount\ quantified\ by\ GC(mol)}{Theoretically\ Produced\ PTDB\ amount\ (mol)} \times 100\%$$

$$DMT\ Yield\ (\%) = \frac{DMT\ amount\ quantified\ by\ GC(mol)}{Theoretically\ Produced\ DMT\ amount\ (mol)} \times 100\%$$

Ex-situ EG capturing process

PET powder (1 mmol), [EMIm][OAc] (5% mol), and MeOH (3 mL) were combined in a polytetrafluoroethylene rotor (25 mL), which was then hermetically sealed within a stainless-steel reactor (C-MAG HS 7C S025 (IKA, Germany, 220~230V, 50/60 Hz, 1020 W)). The reactor was stirred at 180°C for 1.5 hours with a rotational speed of 500 r/min on the heating plate. Following the completion of the reaction, the system was quenched by transferring the reactor into an ice bath. In succession, PTBA (1 mmol) was added to the reaction solution and reacted for 15 min at room temperature. Subsequently, the resulting reaction solution was diluted with 3 mL of trichloromethane. The liquid products were subjected to rotary evaporation to remove solvent, and the remaining solid products were then analyzed via ^{1}H NMR yield, using mesitylene (1 mmol) as an internal standard. The ^{1}H NMR of reaction mixture after ex-situ EG capturing process and the simple examples of DMT separation process was illustrated as Fig. S2 and S3, respectively. The ^{1}H NMR yield of PTDB and DMT were calculated using the following equation:

$$PTDB\ Yield\ (\%) = \frac{PTDB\ \ amount\ quantified\ by\ H\ NMR\ (mol)}{Theoretically\ Produced\ PTDB\ amount\ (mol)} \times 100\%$$

$$DMT\ Yield\ (\%) = \frac{DMT\ amount\ quantified\ by\ H\ NMR\ (mol)}{Theoretically\ Produced\ DMT\ amount\ (mol)} \times 100\%$$

The depolymerization process was extended to various other polyesters, such as poly(ethylene succinate) (PES), poly(ethylene adipate) (PEA), polyethylene 2,5-furandicarboxylate (PEF), and poly(propylene carbonate) (PPC), employing the same method used for the depolymerization of PET.

1.3. Characterizations

^{1}H NMR and ^{13}C NMR spectra were recorded at room temperature using a Bruker Avance-600 instruments (^{1}H NMR at 600 MHz and ^{13}C NMR at 151 MHz), NMR spectra of all products were reported in ppm with reference to solvent signals [^{1}H NMR: $CD(H)Cl_3$ (7.26 ppm), ^{13}C NMR: $CD(H)Cl_3$ (77.00 ppm)]. Signal patterns are indicated as s, singlet; d, doublet; dd, doublets of doublet; t, triplet, and m, multiplet.

The product yield was analyzed by Gas chromatography (GC): Agilent 8860 with Agilent J&W HP-5 Polysiloxane GC Column and Gas chromatography-mass spectrometry (GC-MS): Agilent 7890A/5975C GC/MSD with Agilent J&W HP-5 Polysiloxane GC Column.

The DRIFT spectra were recorded at a spectral resolution of 2 cm^{-1} using a Nicolet iS20 FT-IR spectrometer (Thermo Fisher Scientific). The FT-IR spectra of [EMIm][OAc] with methanol or EG at different ratios were recorded by using a quartz IR cell sealed with CaF_2 windows connected with a vacuum system.

1.4. Methanolysis of PET using different catalysts.

Table S1. Methanolysis of PET with reported catalysts.

Entry	Catalysts	Co-solvent	Temp. (℃)	T (h)	Conv. (%)	Yield (%)	Ref.
1	CO_2	-	220	0.83	100	79.1	1
2	AlP	Toluene	200	2	-	88.5	2
3	$Pb(AC)_2$+ $Zn(AC)_2$	-	120	2	97.8	97.8	3
4	ZnO nanodispersions	-	170	0.25	97	95	4
5	K_2CO_3	DCM	25	24	100	93.1	5
6	Orange peel ash		200	1	-	79	6
7	OPA@Fe_2O_3	-	200	1	100	83	7
8	LiOMe	DMC	65	5	-	91	8
9	Bamboo leaf ash	-	200	2	100	78	9
10	$Ti_{0.5}Si_{0.5}O_2$	-	160	2	100	98.2	10
11	Calcined sodium silicate	-	200	0.5	100	95	11
12	MgO/NaY	-	200	0.5	99	91	12
13	$ChCl/Zn(OAc)_2$	MeCN	170	1	100	90.1	13
14	[HDBU][Im]	-	140	3	100	75	14
15	PIL-Zn^{2+}	-	170	1	100	90.3	15
16	$[HO_3S\text{-}(CH_2)_3\text{-}NEt_3]Cl[ZnCl_2]_{0.67}$	-	195	0.5	-	78.4	16
17	DBN/Phenol	-	130	1	100	95.3	17
18	[BMIm][OAc]	-	150	4	88.5	41.7	18
19	[EMIm][OAc]	-	180	1.5	100	99	This work

Various homogeneous and heterogeneous catalysts have been utilized in the methanolysis of PET. The related literature and partial reaction parameters are summarized in Table S1. Among the diverse catalytic strategies, it is apparent that the yield of DMT reported in most studies is below 95%. The primary products are typically DMT and EG, with limited strategies aimed at the upgrading of EG. In our boronic acid involved EG valorization strategy, we achieve not only complete conversion of PET but also the production of two value-added products, DMT and borate ester, in a one-pot process, yielding 99% and 88%, respectively.

2. Optimization of reaction conditions of in-situ EG capturing strategy

Table S2. Optimization of reaction conditions.

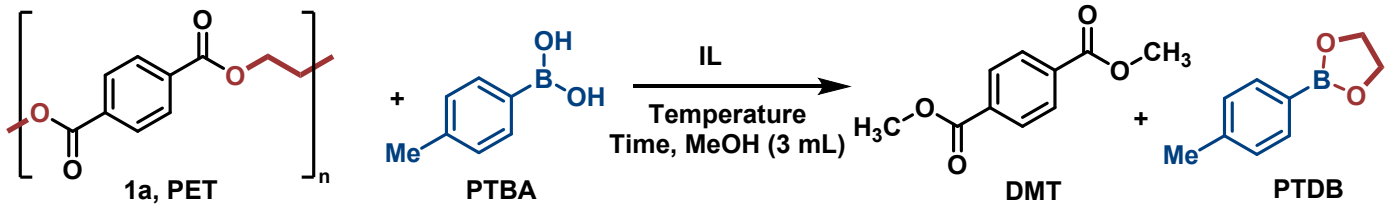

Entry	Cat.	Cat. load.	Temp.	PTBA Conv. (%)	PTDB Yield (%)	DMT Yield (%)	By-product Tol Yield (%)
1	-	-	180 °C	10	9	11	16
1	[EMIm][Cl]	10 mol%	180 °C	23	8	4	15
2	[EMIm][Br]	10 mol%	180 °C	10	4	1	6
4	[EMIm][I]	10 mol%	180 °C	18	4	2	14
5	[EMIm][$MeSO_3$]	10 mol%	180 °C	-	2	<1	-
6	[EMIm][BF_4]	10 mol%	180 °C	71	2	<1	69
7	[EMIm][OAc]	10 mol%	180 °C	100	86	99	14
8	[BMIm][OAC]	10 mol%	180 °C	100	84	99	16
9	[EMIm][OAc]	15 mol%	180 °C	100	80	99	20
10	[EMIm][OAc]	5 mol%	180 °C	100	88	99	12
11	[EMIm][OAc]	2 mol%	180 °C	100	86	91	14
12	[EMIm][OAc]	5 mol%	160 °C	100	91	86	9
13	[EMIm][OAc]	5 mol%	200 °C	100	55	99	45

[a]Standard reaction conditions: PET (1 mmol), PTBA (1 mmol) and MeOH (3 mL) at 180 °C for 1.5 h. Yields were determined by GC analyses with mesitylene as internal standard.

Initially, the absence of ILs led to minimal PET depolymerization and EG esterification, resulting in only 8% DMT and 9% PTDB after heating at 180℃ for 1.5 hours (Table S2, entries 1). Subsequently, $[EMIm]^+$-based ionic ILs with various anions ([EMIm][Cl], [EMIm][Br], [EMIm][I], [EMIm][$MeSO_3$], [EMIm][BF_4], and [EMIm][OAc]) were chosen for PET depolymerization under metal-free condition. The related studies reported that $[OAc]^-$ has a relatively stronger H-bond acceptance compared to other anions ($[MeSO_3]^-$, $[X]^-$, and $[BF_4]^-$).[19-22] It was observed that only basic [EMIm][OAc], with a stronger H-bond acceptance capacity, exhibited outstanding catalytic performance in both PET depolymerization and EG esterification processes (entries 2-7).[20] Other ILs tested did not effectively catalyze the degradation of PET and resulted in undesired protodeboronation of PTBA. This result emphasizes the crucial role of the $[OAc]^-$ in this PET valorization process. Subsequently, the increased basicity of [BMIm][OAc] by modifying the alkyl chain length of the cations leads to more toluene byproduct formation due to the protodeboronation of PTBA (Ar-B → Ar-H) (entry 8).[20, 21, 23, 24]This finding indicated the significant role of the basic intensity of ILs for EG esterification with PTBA. In addition, an increased catalyst loading promotes the protodeboronation of PTBA, while decreasing the catalyst loading to 5 mol% achieves the yields of 88% PTDB and 99% DMT, respectively

(entry 9-10). However, the further lowering catalyst loading resulted in insufficient PET degradation (entry 11). Subsequently, increasing or decreasing the system temperature were also performed, but failed to provide improved yields of either PTDB or DMT (entry 12-13). Additionally, the time curve of PET valorization process was also analyzed as described in Fig. S1b.

3. Reaction kinetics studies and product separation

3.1 kinetics studies

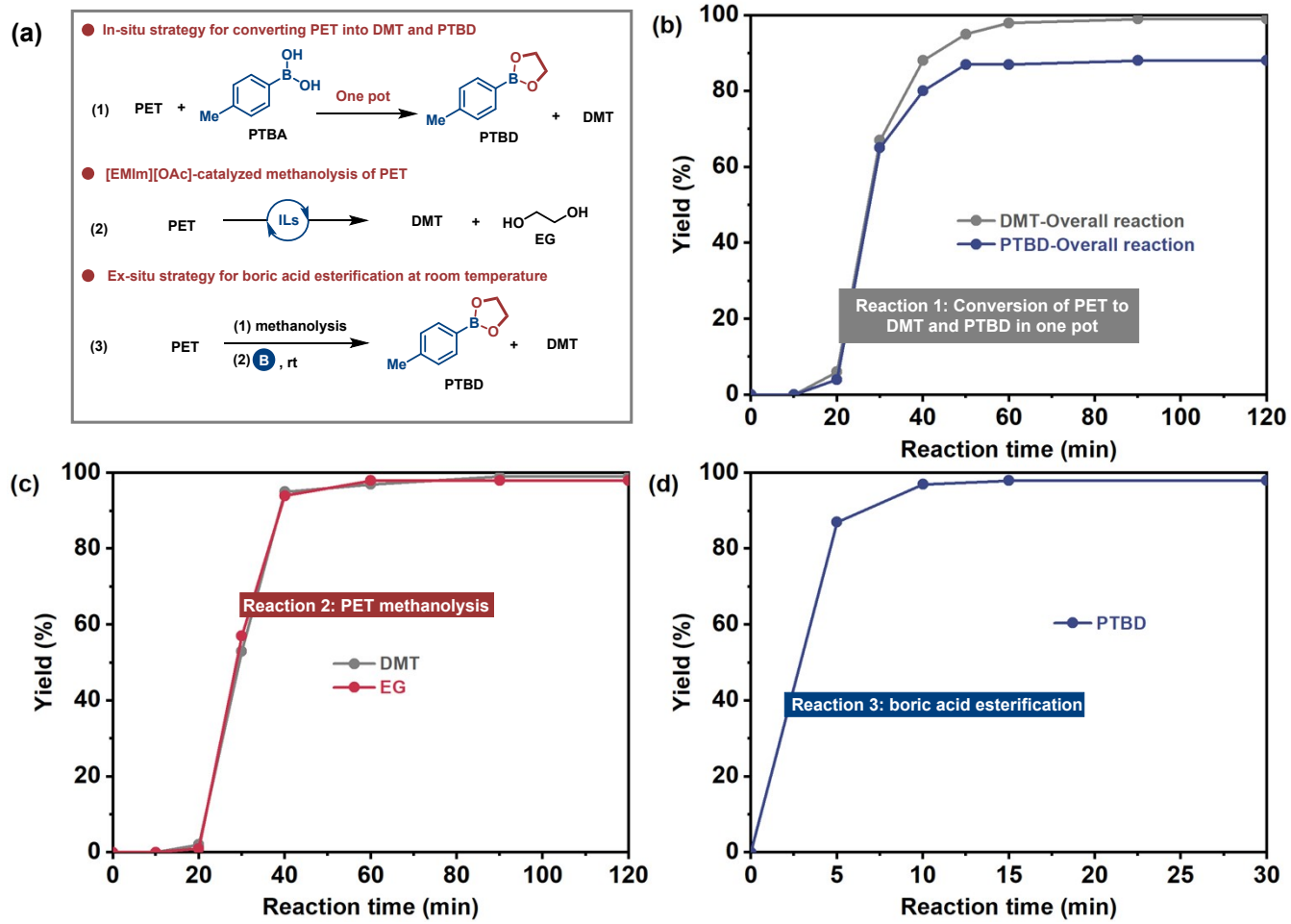

Fig. S1. Kinetic studies. (a) Different the reaction pathway. (b) Time curve of the overall reaction. (c) Time curve of the sole PET methanolysis. (d) Time curve of the PTBA esterification in the reaction mixture at room temperature after PET methanolysis. Standard reaction conditions of 1: PET (1 mmol), PTBA (1 mmol), [EMIm][OAc] (5 mol%), and MeOH (3 mL) at 180°C. Conditions of reaction 2: PET (1 mmol), [EMIm][OAc] (5 mol%), and MeOH (3 mL) at 180°C. Conditions of reaction 3: step 1: PET (1 mmol), [EMIm][OAc] (5 mol%) and MeOH (3 mL) at 180°C. step 2: adding PTBA (1 mmol) to the reaction mixture at room temperature after PET methanolysis. Yield was determined by ^{1}H NMR.

To comprehend the reaction pathway, we examined the reaction kinetics. The time curve of different reaction pathway (overall reaction, PET methanolysis and PTBA esterification) were analyzed (Fig. S1a). The one-pot production of PTBD and DMT delivering from PET involves the methanolysis of PET and the subsequent esterification of EG with PTBA. The results indicated that the yields of PTBD and DMT steadily increase throughout the reaction, peaking at 88% and 99%, respectively, after 1.5 hours (Fig. S1b). Interestingly, no EG monomer was observed during the reaction, indicating that PTBA is an effective EG valorization reagent in this in-situ EG capturing approach.

Subsequent experiments were conducted with consistent reaction times focusing on sole PET methanolysis (Fig. S1c), resulting in the conversion of PET to 99% DMT and 98% EG within 1.5 hours. PTBA was then added to the reaction solution at room temperature to capture EG and convert it to PTDB with a yield

of 98% within 15 minutes (Fig. S1d). These findings demonstrated the significant promotion effect of [EMIm][OAc] both on PET methanolysis and PTBA esterification.

3.2 ^{1}H NMR of reaction mixture after ex-situ EG capturing process

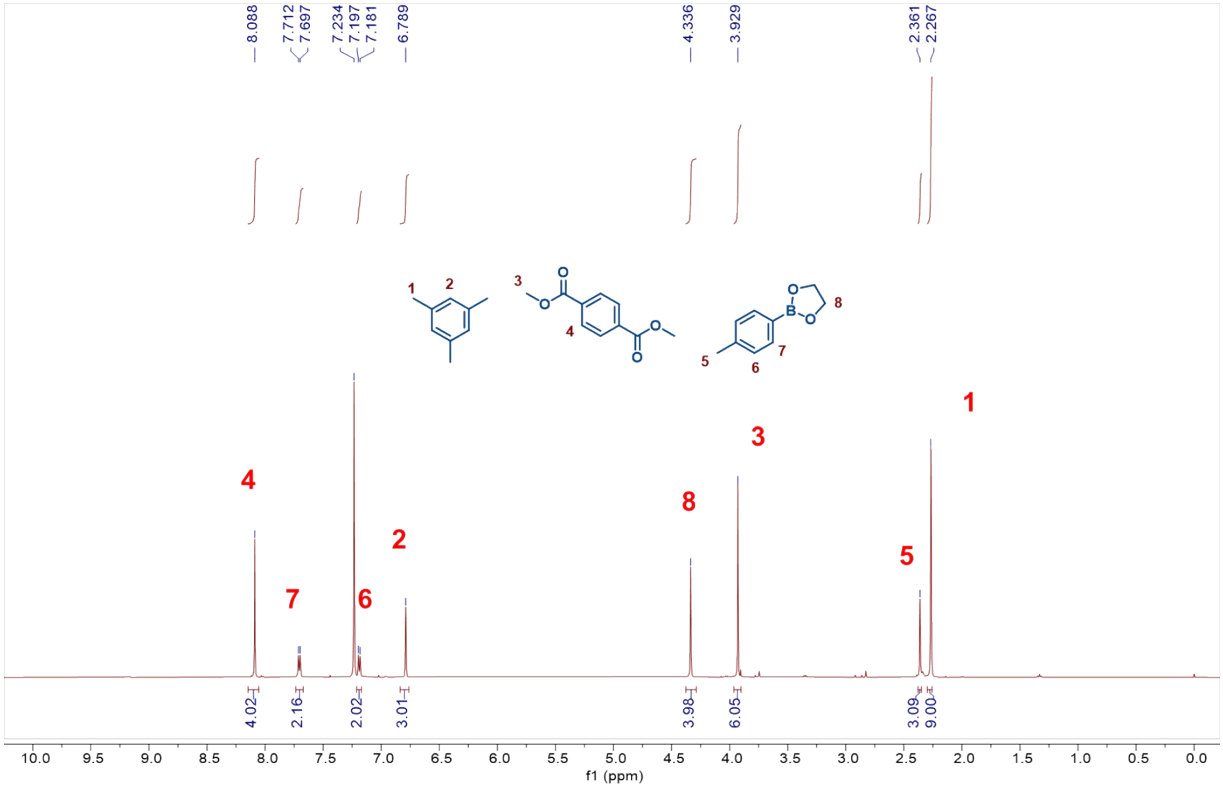

Fig. S2. Reaction conditions: step 1: PET (1 mmol), [EMIm][OAc] (5 mol%) and MeOH (3 mL) at 180°C. step 2: adding PTBA (1 mmol) to the reaction mixture at room temperature after PET methanolysis. Yield was determined by ^{1}H NMR after solvent removal by rotary evaporation..

After the ex-situ EG capturing process, the liquid products were subjected to rotary evaporation to remove solvent, and the remaining solid products were then analyzed via ^{1}H NMR yield. The ^{1}H NMR results indicated that PET and PTBA have been almost fully targeted and transformed into DMT and PTBA respectively, while EG and the by-product toluene from protodeboronation of PTBA are nearly not observed.

3.3 Simple examples of DMT separation process

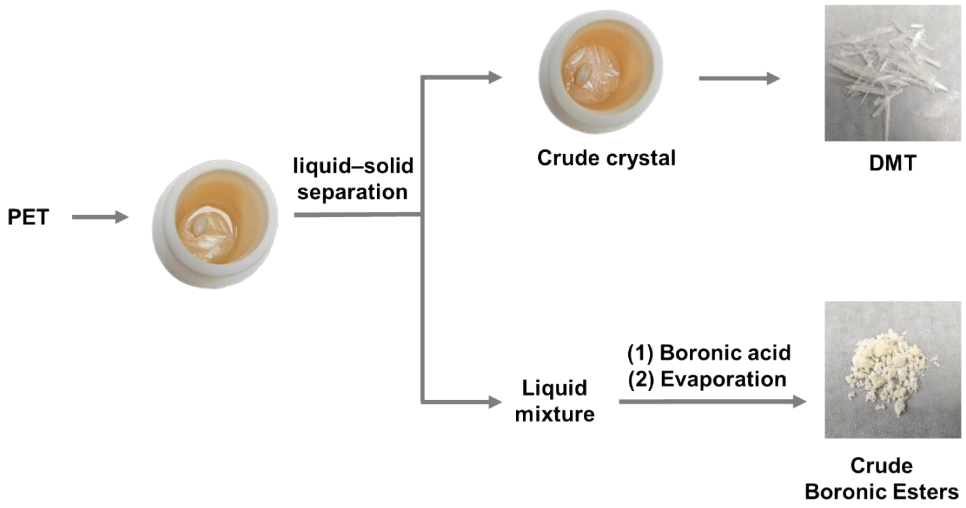

Fig. S3. DMT separation process.

After the reaction, crude DMT crystals were obtained upon cooling. Subsequently, highly pure transparent DMT crystals were harvested through additional washing with cold methanol. Boronic acids were added to the liquid mixture and allowed to react for 15 minutes. Following the completion of the reaction, the methanol was then evaporated to obtain the crude boronic esters.

4. Polyester chemical recycling based on in-situ or ex-situ EG capture strategies

4.1 Substrate adaptability of the in-situ EG capturing strategy

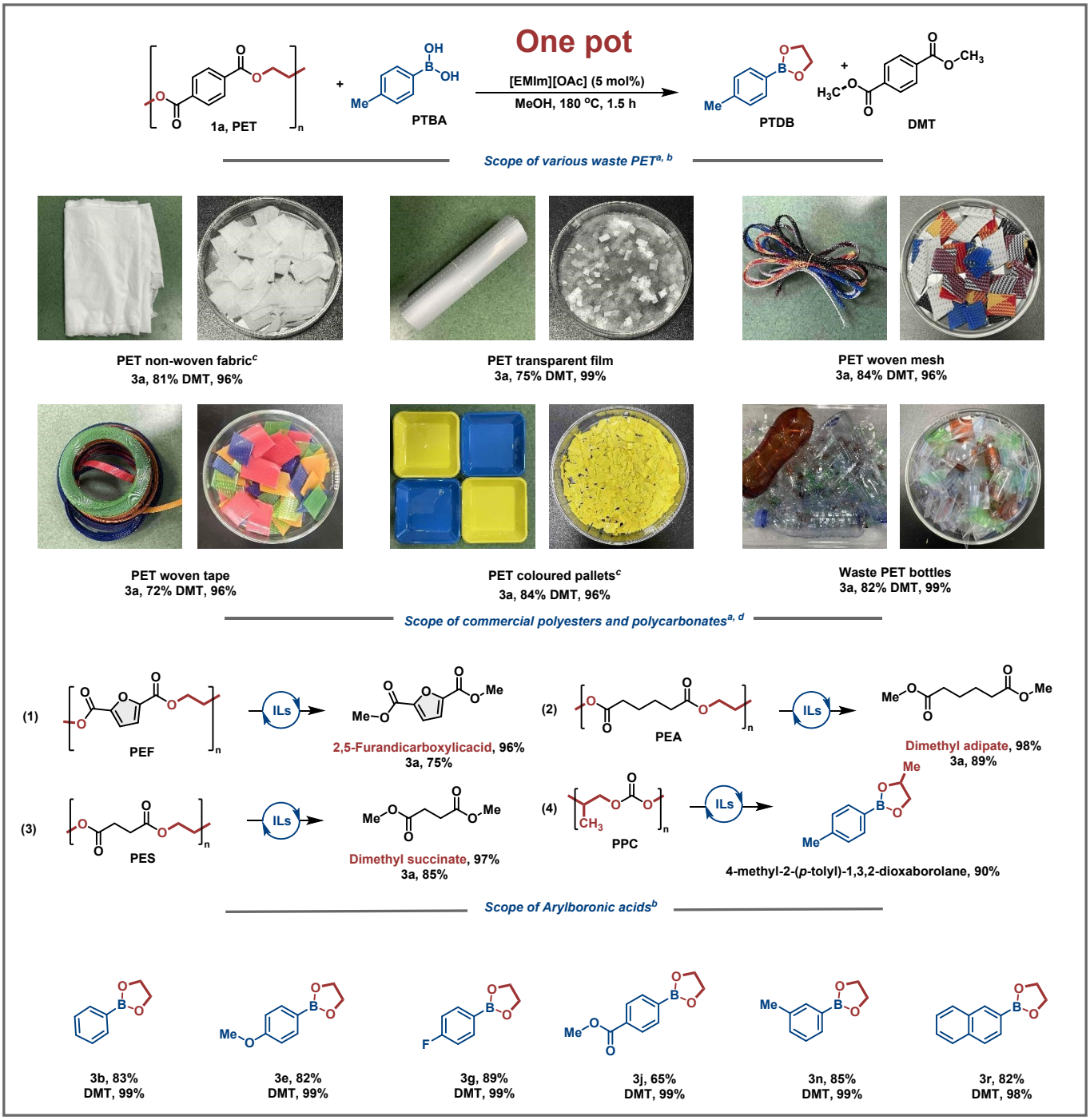

Fig. S4. One-pot conversion of PET to boronic esters and DMT. [a]Standard reaction conditions: polyesters or polycarbonates (1 mmol), boronic acid (1 mmol), [EMIm][OAc] (5 mol%), and MeOH (3 mL) at 180°C for 1.5 h. [b]Yields were determined by GC analyses with mesitylene as internal standard. [c]at 180°C for 3 h. [d]Yields were determined by ^{1}H NMR analyses with mesitylene as internal standard after solvent removal by rotary evaporation.

4.2 Chemical recycling of PET fabrics by the ex-situ EG capturing strategy

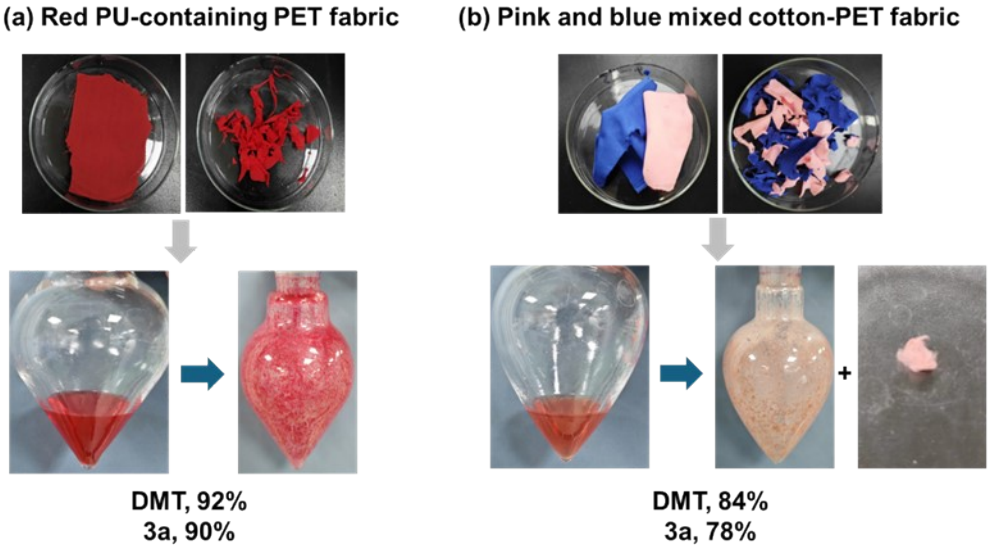

Fig. S5. Changes in the reaction mixture of blending PET fabrics before and after reaction. Standard reaction conditions: (1) polyester (1 mmol), [EMIm][OAc] (5 mol%), and MeOH (3 mL) at 180 °C for 1.5 h. (2) boronic acids (1 mmol) at room temperature for 15 min. Yields were determined by ^{1}H NMR analyses with mesitylene as internal standard after solvent removal by rotary evaporation.

To further validate the feasibility of our ex-situ EG capturing strategy, we conducted chemical recycling of PET-blending fabrics containing different proportions of PU and cotton. The transformations occurring before and after the reaction were illustrated in Fig. S5. The yields of both DMT and 3a were detected by ^{1}H NMR using mesitylene as an internal standard. The 5% PU-containing PET waste fabrics were converted into a dark red solution, yielding DMT and **3a** at 92% and 90% respectively. In contrast, the PET waste that contained cotton was converted into a light pink solution, yielding 84% DMT and 78% **3a**, while simultaneously precipitating solid (insoluble cotton matter). The experimental results indicated that this strategy demonstrates good applicability for colored and impure PET waste.

5. ^{1}H NMR and ^{13}C NMR data of all compounds

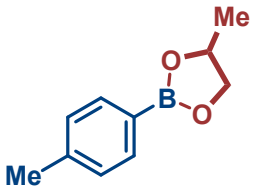

(*S*)-4-methyl-2-(*p*-tolyl)-1,3,2-dioxaborolane[25]: colorless liquid, ^{1}H NMR yield 95%; ^{1}H NMR (600 MHz, $CDCl_3$) δ = 7.70 (d, *J* = 7.8 Hz, 2H), 7.19 (d, *J* = 7.8 Hz, 2H), 4.73-4.67 (m, 1H), 4.43 (dd, *J* = 9.0, 7.8 Hz, 1H), 3.87 (dd, *J* = 9.0, 7.8 Hz, 1H), 2.37 (s, 3H), 1.40 (d, *J* = 6.0 Hz, 3H); ^{13}C NMR (151 MHz, $CDCl_3$) δ = 141.6, 134.8, 128.6, 73.6, 72.5, 21.7.

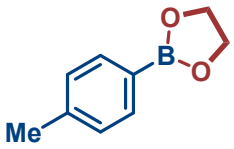

2-(*p*-tolyl)-1,3,2-dioxaborolane 3a[25]: white solid, ^{1}H NMR yield 97%; ^{1}H NMR (600 MHz, $CDCl_3$) δ = 7.71 (d, *J* = 7.8 Hz, 2H), 7.17 (d, *J* = 7.2 Hz, 2H), 4.28 (s, 4H), 2.34 (s, 3H); ^{13}C NMR (151 MHz, $CDCl_3$) δ = 141.5, 134.8, 128.5, 65.8, 21.6.

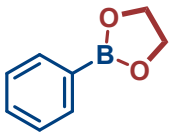

2-phenyl-1,3,2-dioxaborolane 3b[25]: white solid, ^{1}H NMR yield 93%; ^{1}H NMR (600 MHz, $CDCl_3$) δ = 7.82 (d, *J* = 6.6 Hz, 2H), 7.45 (t, *J* = 7.8 Hz, 1H), 7.36 (t, *J* = 7.8 Hz, 2H), 4.29 (s, 4H); ^{13}C NMR (151 MHz, $CDCl_3$) δ = 130.7, 131.3, 127.7, 65.9.

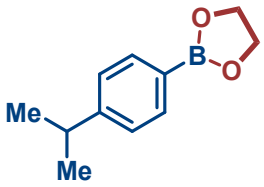

2-(4-isopropylphenyl)-1,3,2-dioxaborolane 3c[26]: white solid, ^{1}H NMR yield 97%; ^{1}H NMR (600 MHz, $CDCl_3$) δ = 7.75 (d, *J* = 7.8 Hz, 2H), 7.24 (d, *J* = 7.8 Hz, 2H), 4.29 (s, 6H), 2.93-2.86 (m, 1H), 1.24 (d, *J* = 7.2 Hz, 6H); ^{13}C NMR (151 MHz, $CDCl_3$) δ = 152.3, 134.9, 125.9, 65.8,34.2, 23.7.

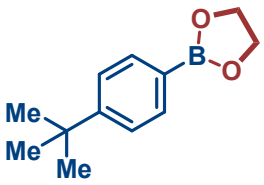

2-(4-(*tert*-butyl)phenyl)-1,3,2-dioxaborolane 3d: white solid, ^{1}H NMR yield 96%; ^{1}H NMR (600 MHz, $CDCl_3$) δ = 7.76 (d, *J* = 8.4 Hz, 2H), δ = 7.41 (d, *J* = 8.4 Hz, 2H), 4.32 (s, 4H) , 1.32 (s, 9H); ^{13}C NMR (151 MHz, $CDCl_3$) δ = 154.6, 134.7, 124.7, 65.8, 34.8, 31.1.

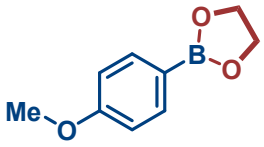

2-(4-methoxyphenyl)-1,3,2-dioxaborolane 3e[25]: white solid, ^{1}H NMR yield 98%; ^{1}H NMR (600 MHz, $CDCl_3$) δ = 7.75 (d, *J* = 8.4 Hz, 2H), 6.90 (d, *J* = 8.4 Hz, 2H), 4.03 (s, 4H), 3.79 (s, 3H); ^{13}C NMR (151 MHz, $CDCl_3$) δ = 162.2, 136.5, 113.3, 65.8, 54.9.

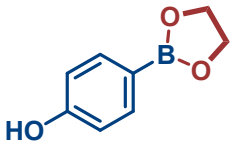

4-(1,3,2-dioxaborolan-2-yl)phenol 3f[27]: white solid, ^{1}H NMR yield 92%; ^{1}H NMR (600 MHz, $CDCl_3$) δ = 7.70 (d, *J* = 7.2 Hz, 2H), 6.90 (d, *J* = 8.4 Hz, 2H), 4.34 (s, 4H), 3.73 (s, 1H); ^{13}C NMR (151 MHz, $CDCl_3$) δ = 158.8, 136.8, 115.0, 65.8.

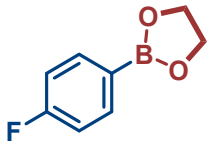

2-(4-fluorophenyl)-1,3,2-dioxaborolane 3g[25]: white solid, ^{1}H NMR yield 97%; ^{1}H NMR (600 MHz, $CDCl_3$) δ = 7.81-7.79 (m, 2H), 7.05 (t, *J* = 9.0 Hz, 2H), 4.31 (s, 4H); ^{13}C NMR (151 MHz, $CDCl_3$) δ = 165.1 (d, *J* = 250.8 Hz), 137.0 (d, *J* = 8.2 Hz), 114.9 (d, *J* = 20.4 Hz), 65.9.

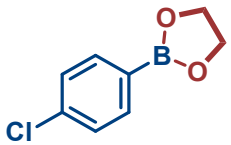

2-(4-chlorophenyl)-1,3,2-dioxaborolane 3h[28]: white solid, ^{1}H NMR yield 98%; ^{1}H NMR (600 MHz, $CDCl_3$) δ = 7.71 (d, *J* = 7.8 Hz, 2H), 7.33 (d, *J* = 7.8 Hz, 2H), 4.30 (s, 4H); ^{13}C NMR (151 MHz, $CDCl_3$) δ = 137.6, 136.1, 128.0, 65.9.

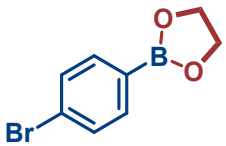

2-(4-bromophenyl)-1,3,2-dioxaborolane 3i[29]: white solid, ^{1}H NMR yield 97%; ^{1}H NMR (600 MHz, $CDCl_3$) δ = 7.65 (d, *J* = 8.4 Hz, 2H), 7.51 (d, *J* = 7.8 Hz, 2H), 4.33 (s, 4H); ^{13}C NMR (151 MHz, $CDCl_3$) δ = 136.3, 131.0, 126.4, 66.0.

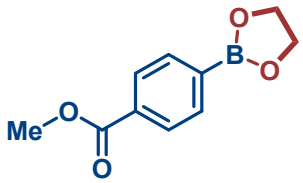

Methyl 4-(1,3,2-dioxaborolan-2-yl)benzoate 3j[25]: white solid, ^{1}H NMR yield 97%; ^{1}H NMR (600 MHz, $CDCl_3$) δ = 8.04 (d, *J* = 8.4 Hz, 2H), 7.88 (d, *J* = 8.4 Hz, 2H), 4.40 (s, 4H), 3.92 (s, 3H); ^{13}C NMR (151 MHz, $CDCl_3$) δ = 167.0, 134.7, 132.5, 128.7, 66.2, 52.2.

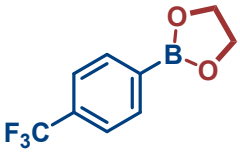

2-(4-(trifluoromethyl)phenyl)-1,3,2-dioxaborolane 3k[28]: white solid, ^{1}H NMR yield 92%; ^{1}H NMR (600 MHz, $CDCl_3$) δ = 7.90 (d, *J* = 7.8 Hz, 2H), 7.61 (d, *J* = 8.4 Hz, 2H), 4.35 (s, 4H); ^{13}C NMR (151 MHz, $CDCl_3$) δ = 135.1, 132.9 (q, *J* = 32.2 Hz), 124.4 (q, *J* = 3.5 Hz), 124.1 (q, *J* = 272.6 Hz), 66.1.

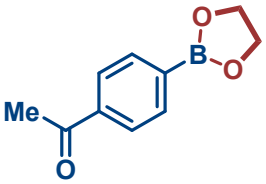

1-(4-(1,3,2-dioxaborolan-2-yl)phenyl)ethan-1-one 3l[30]: white solid, ^{1}H NMR yield 95%; ^{1}H NMR (600 MHz, $CDCl_3$) δ = 7.93 (d, *J* = 7.8 Hz, 2H), 7.88 (d, *J* = 7.8 Hz, 2H), 4.38 (s, 4H), 2.60 (s, 3H); ^{13}C NMR (151 MHz, $CDCl_3$) δ = 198.2, 134.8, 127.2, 66.0, 26.5.

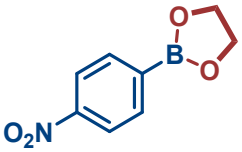

2-(4-nitrophenyl)-1,3,2-dioxaborolane 3m[31]: white solid, ^{1}H NMR yield 94%; ^{1}H NMR (600 MHz, $CDCl_3$) δ = 8.20 (d, *J* = 8.4 Hz, 2H), 7.96 (d, *J* = 8.4 Hz, 2H), 4.44 (s, 4H); ^{13}C NMR (151 MHz, $CDCl_3$) δ = 149.9, 135.7, 122.5, 66.4.

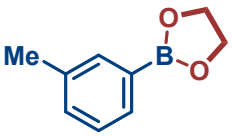

2-(*m*-tolyl)-1,3,2-dioxaborolane 3n[32]: white solid, ^{1}H NMR yield 98%; ^{1}H NMR (600 MHz, $CDCl_3$) δ = 7.64 (s, 1H),7.62-7.60 (m, 1H), 7.28-7.26 (m, 2H), 4.33 (s, 4H), 2.35 (s, 3H); ^{13}C NMR (151 MHz, $CDCl_3$) δ = 137.1, 135.4, 132.2, 131.8, 127.7, 65.9, 21.2.

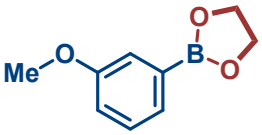

2-(3-methoxyphenyl)-1,3,2-dioxaborolane 3o[29]: white solid, ^{1}H NMR yield 95%; ^{1}H NMR (600 MHz, $CDCl_3$) δ = 7.40 (d, *J* = 6.6 Hz, 1H), 7.33 (d, *J* = 1.8 Hz, 1H), 7.28 (t, *J* = 7.8 Hz, 1H), 7.00-6.99 (m, 1H), 4.28 (s, 4H), 3.77 (s, 3H); ^{13}C NMR (151 MHz, $CDCl_3$) δ = 158.9, 128.9, 127.0, 118.8, 117.6, 65.8, 54.9.

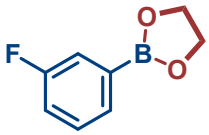

2-(3-fluorophenyl)-1,3,2-dioxaborolane 3p[33]: white solid, ^{1}H NMR yield 95%; ^{1}H NMR (600 MHz, $CDCl_3$) δ = 7.57 (d, *J* = 6.6 Hz, 1H), 7.33 (dd, *J* = 9.0 Hz, 1.8 Hz, 1H), 7.34-7.31 (m, 1H), 7.15-7.12 (m, 1H), 4.32 (s, 4H); ^{13}C NMR (151 MHz, CDCl3) δ = 162.4 (d, *J* = 246.4 Hz), 130.3 (d, *J* = 3.0 Hz), 129.5 (d, *J* = 7.2 Hz), 120.9 (d, *J* = 19.5 Hz), 118.3 (d, *J* = 21.0 Hz), 66.0.

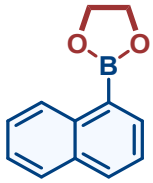

2-(naphthalen-1-yl)-1,3,2-dioxaborolane 3q[29]: white solid, ^{1}H NMR yield 94%; ^{1}H NMR (600 MHz, $CDCl_3$) δ = 8.74 (d, *J* = 8.4 Hz, 1H), 8.11 (d, *J* = 5.4 Hz, 1H), 7.94 (d, *J* = 8.4 Hz, 1H), 7.83 (d, *J* = 7.8 Hz, 1H), 7.54-7.52 (m, 1H), 7.48-7.45 (m, 2H), 4.42 (s, 3H); ^{13}C NMR (151 MHz, $CDCl_3$) δ = 136.8, 136.1, 133.2, 131.9, 128.4, 128.2, 126.4, 125.5, 124.9, 65.9.

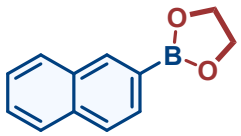

2-(naphthalen-2-yl)-1,3,2-dioxaborolane 3r[25]: white solid, ^{1}H NMR yield 95%; ^{1}H NMR (600 MHz, $CDCl_3$) δ = 8.37 (s, 1H), 8.37-7.79 (m, 4H), 7.47-7.42 (m, 2H), 4.27 (s, 3H); ^{13}C NMR (151 MHz, $CDCl_3$) δ = 136.4, 135.0, 132.7, 130.2, 128.6, 127.6, 127.0, 127.0, 125.8, 65.9.

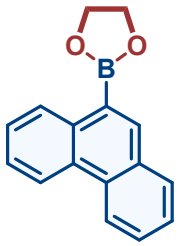

2-(phenanthren-9-yl)-1,3,2-dioxaborolane 3s[34]: white solid, ^{1}H NMR yield 91%; ^{1}H NMR (600 MHz, $CDCl_3$) δ =8.81-8.79 (m, 1H), 8.69-8.64 (m, 2H), 8.42 (s, 1H), 7.91 (d, *J* = 7.2 Hz, 1H), 7.68-7.56 (m, 4H), 4.44 (s, 4H); ^{13}C NMR (151 MHz, $CDCl_3$) δ = 138.8, 134.3, 132.0, 130.9, 129.9, 129.4, 128.9, 127.9, 126.7, 126.5, 126.2, 122.6, 122.5, 65.9.

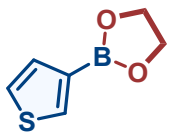

2-(thiophen-3-yl)-1,3,2-dioxaborolane 3t[35]: white solid, ^{1}H NMR yield 93%; ^{1}H NMR (600 MHz, $CDCl_3$) δ = 7.93 (d, *J* = 1.8 Hz, 1H), 7.40 (d, *J* = 3.6 Hz, 1H), 7.32 (dd, *J* = 4.8, 2.4 Hz, 1H), 4.27 (s, 4H); ^{13}C NMR (151 MHz, $CDCl_3$) δ = 136.6, 131.8, 125.4, 65.7.

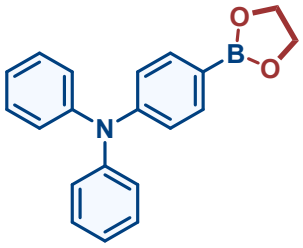

4-(1,3,2-dioxaborolan-2-yl)-*N*,*N*-diphenylaniline 3u[36]: white solid, ^{1}H NMR yield 94%; ^{1}H NMR (600 MHz, $CDCl_3$) δ = 7.65 (d, *J* = 8.4 Hz, 2H), 7.25 (t, *J* = 8.4 Hz, 4H), 7.12-7.10 (m, 4H), 7.06-7.01 (m, 4H), 4.32 (s, 4H); ^{13}C NMR (151 MHz, $CDCl_3$) δ = 150.7, 147.2, 135.9, 129.3, 125.1, 123.5, 121.3, 65.9.

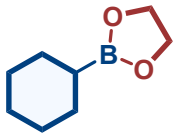

2-cyclohexyl-1,3,2-dioxaborolane 3v[37]: white solid, ^{1}H NMR yield 83%; ^{1}H NMR (600 MHz, $CDCl_3$) δ = 4.17 (s, 4H), 1.72-1.60 (m, 5H), 1.35-1.28 (m, 5H), 1.07-1.03 (m, 1H); ^{13}C NMR (151 MHz, $CDCl_3$) δ = 65.4, 28.0, 27.2, 26.7

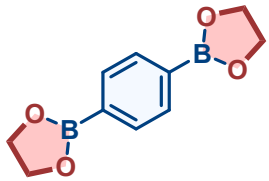

1,4-di(1,3,2-dioxaborolan-2-yl)benzene 3w[36]: white solid, ^{1}H NMR yield 93%; ^{1}H NMR (600 MHz, $CDCl_3$) δ = 8.08 (s, 4H), 3.92 (s, 8H); ^{13}C NMR (151 MHz, $CDCl_3$) δ = 134.1, 66.1.

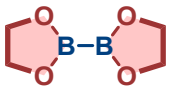

2,2'-bi(1,3,2-dioxaborolane) 3x[27]: white solid, ^{1}H NMR yield 65%; ^{1}H NMR (600 MHz, $CDCl_3$) δ = 4.21 (s, 8H); ^{13}C NMR (151 MHz, $CDCl_3$) δ = 65.3.

6. ^{1}H NMR and ^{13}C NMR spectra of all compounds

^{1}H NMR of (*S*)-4-methyl-2-(*p*-tolyl)-1,3,2-dioxaborolane (600 MHz, $CDCl_3$) and ^{13}C NMR of (*S*)-4-methyl-2-(*p*-tolyl)-1,3,2-dioxaborolane (151 MHz, $CDCl_3$)

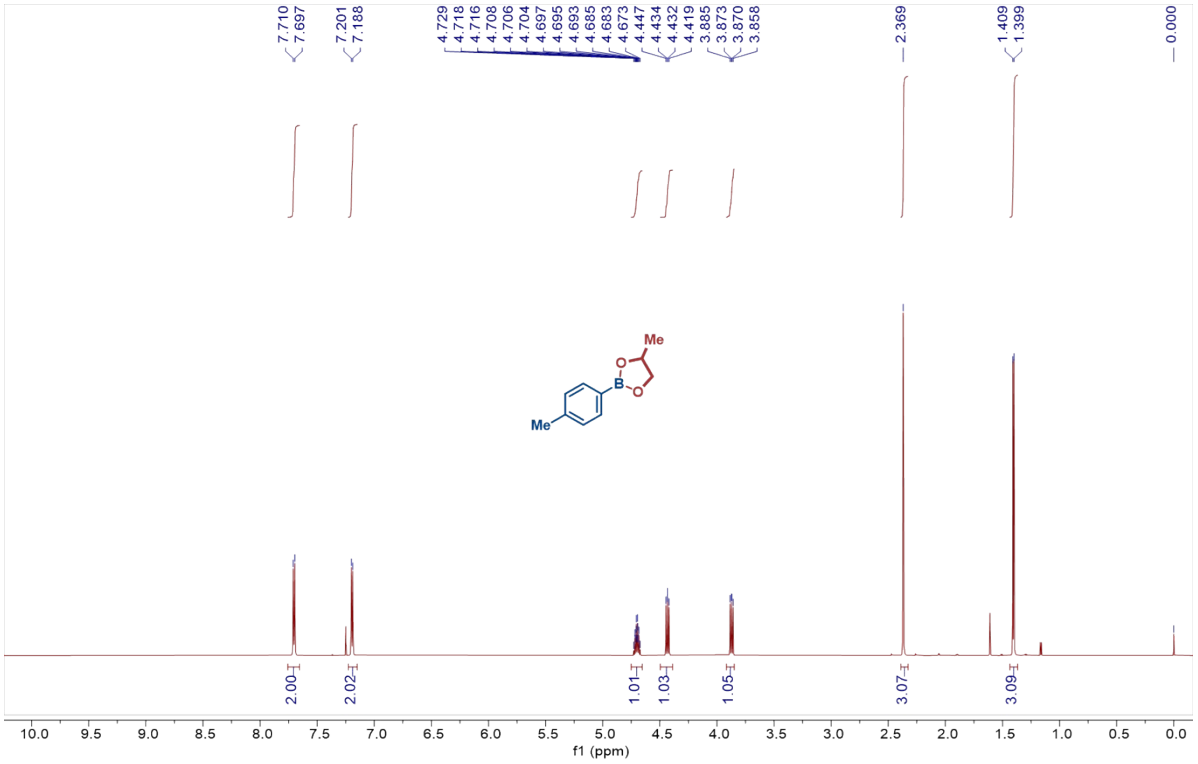

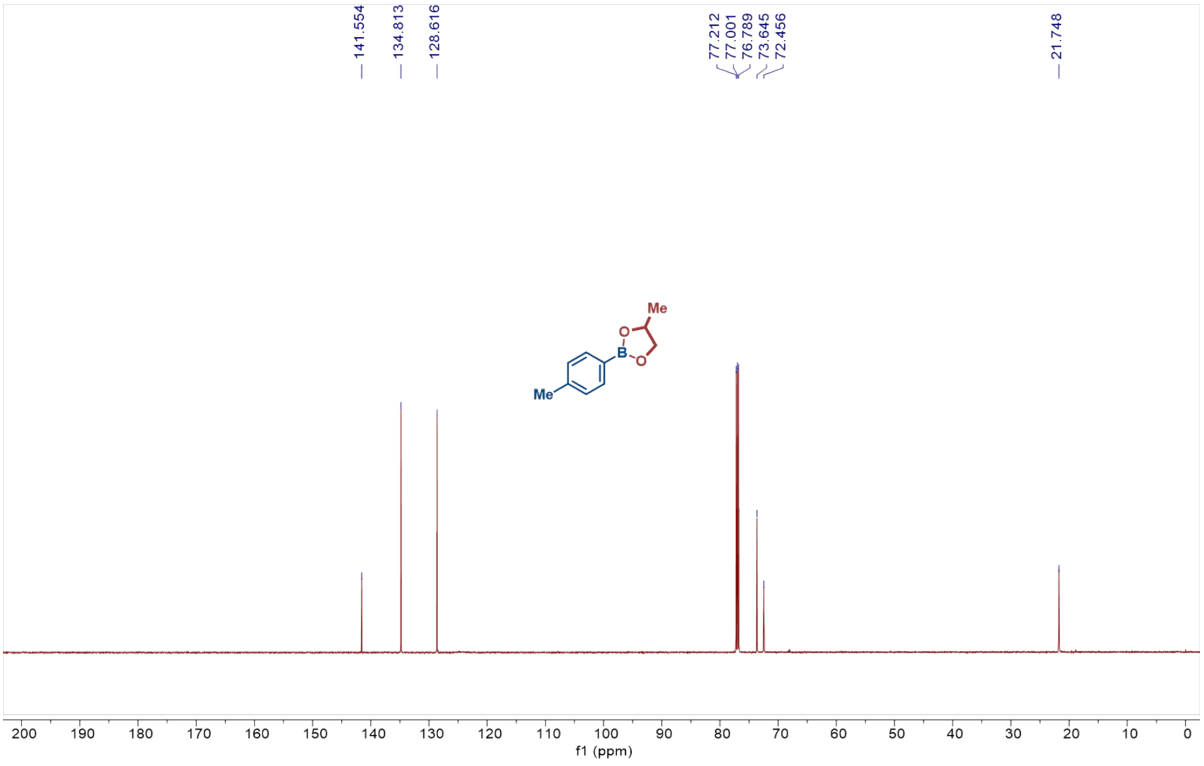

^{1}H NMR of **3a** (600 MHz, $CDCl_3$) and ^{13}C NMR of **3a** (151 MHz, $CDCl_3$)

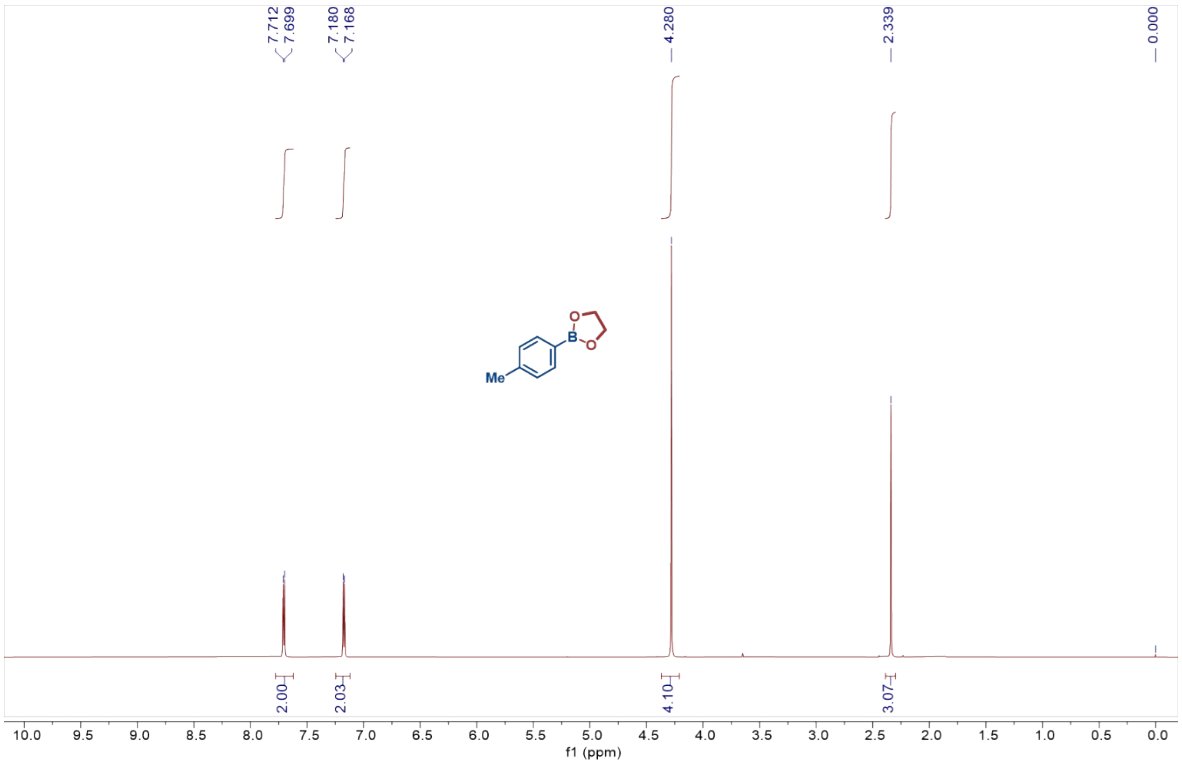

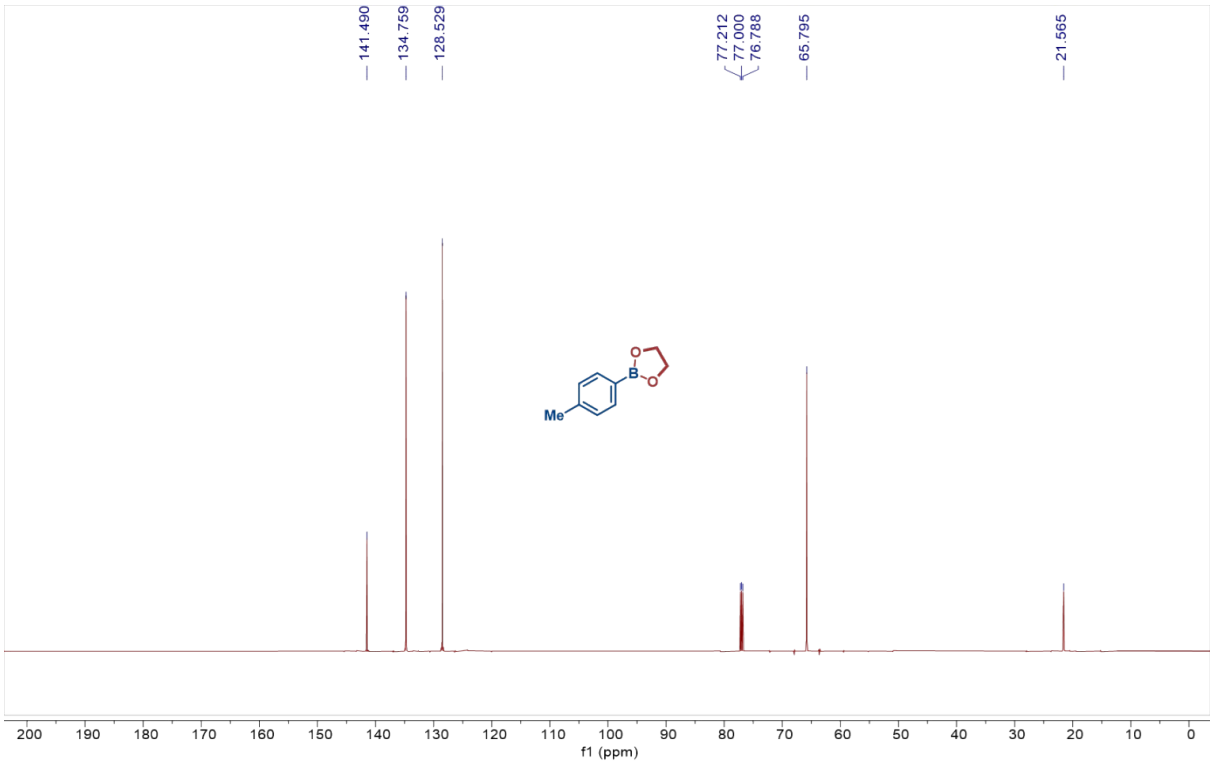

^{1}H NMR of **3b** (600 MHz, $CDCl_3$) and ^{13}C NMR of **3b** (151 MHz, $CDCl_3$)

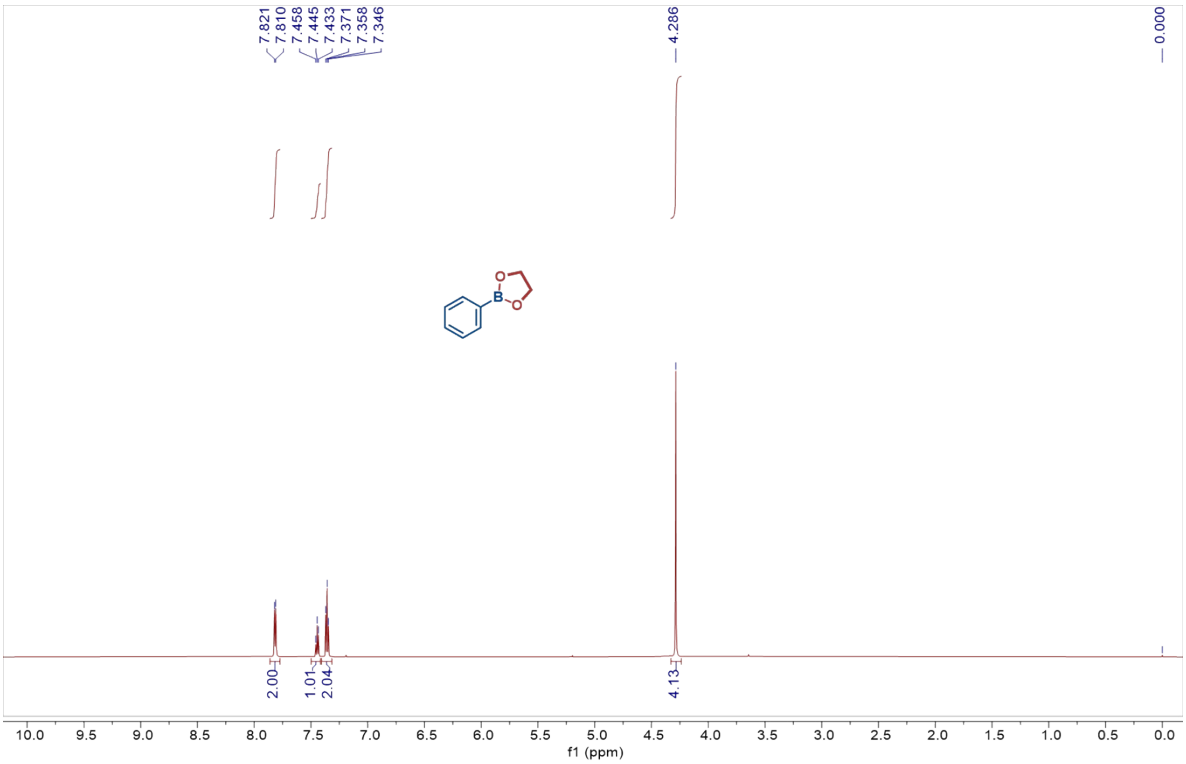

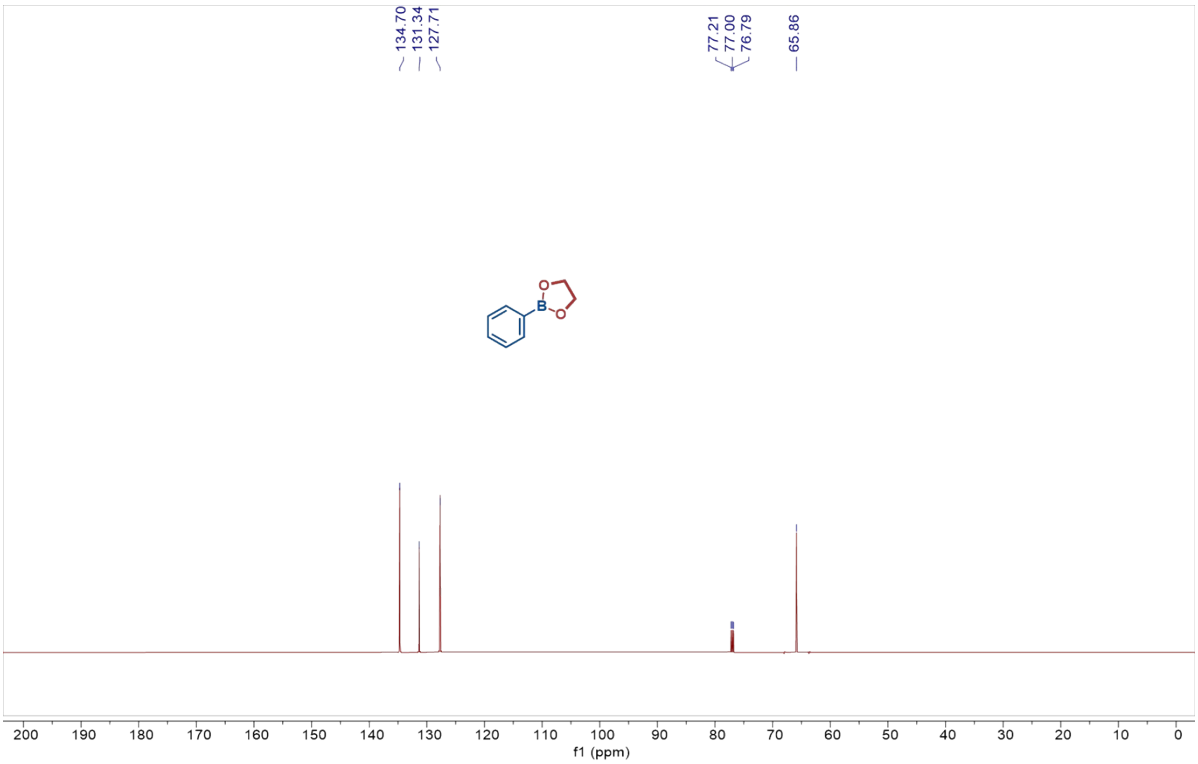

^{1}H NMR of **3c** (600 MHz, $CDCl_3$) and ^{13}C NMR of **3c** (151 MHz, $CDCl_3$)

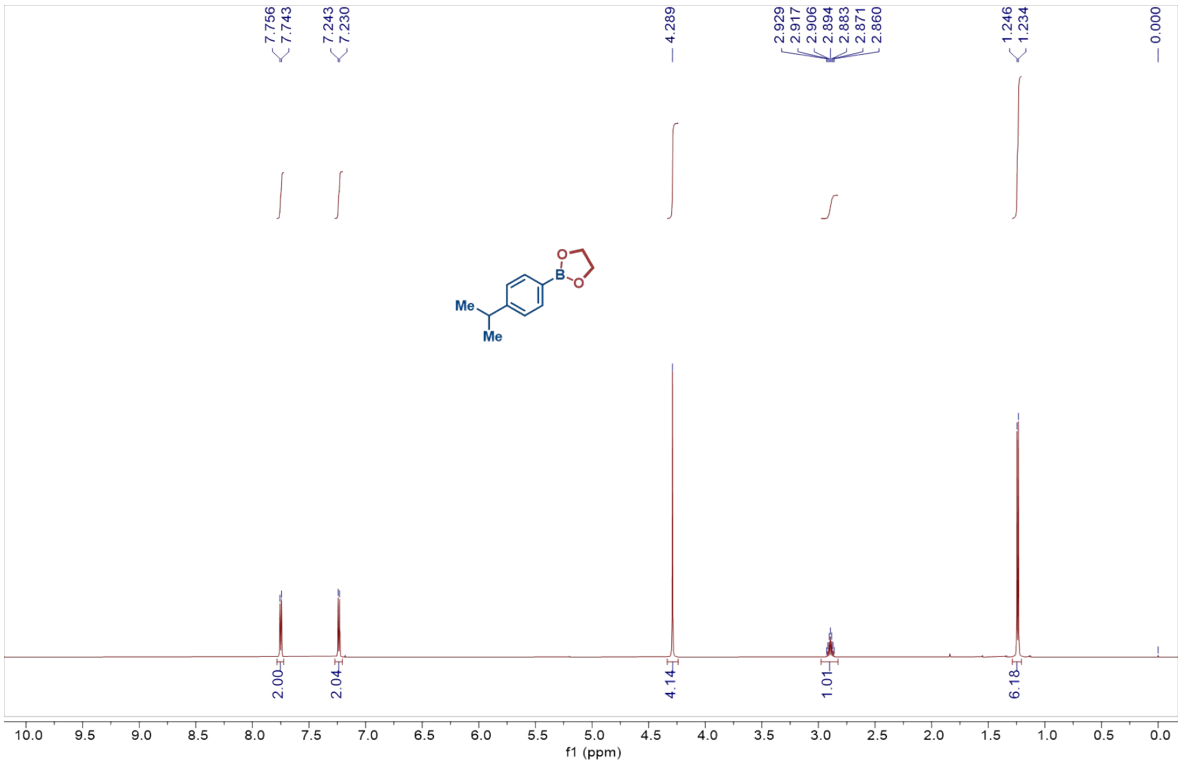

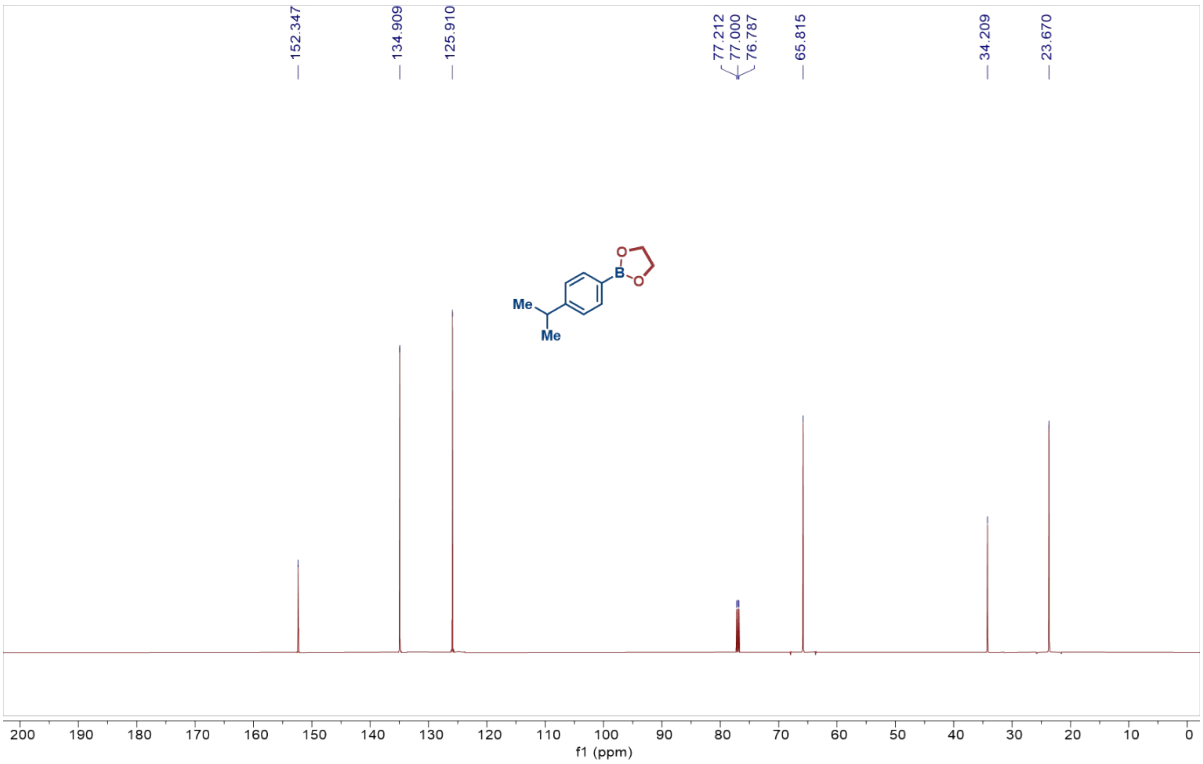

^{1}H NMR of **3d** (600 MHz, $CDCl_3$) and ^{13}C NMR of **3d** (151 MHz, $CDCl_3$)

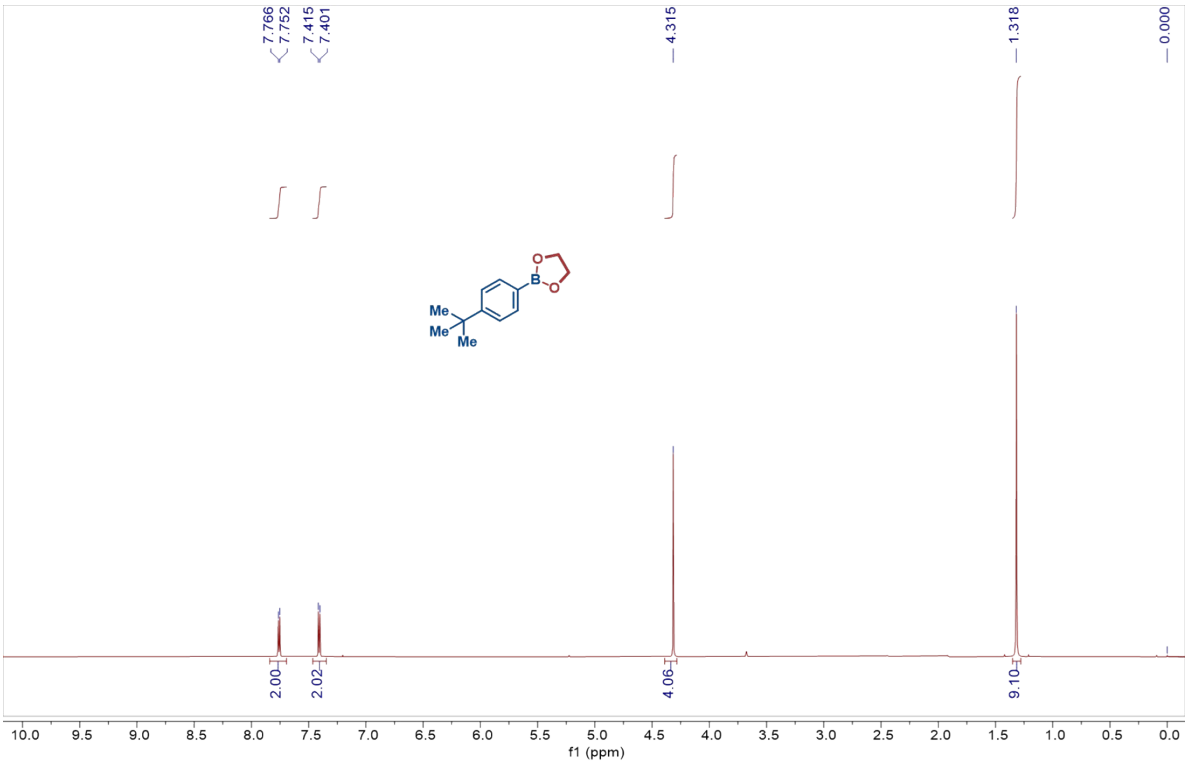

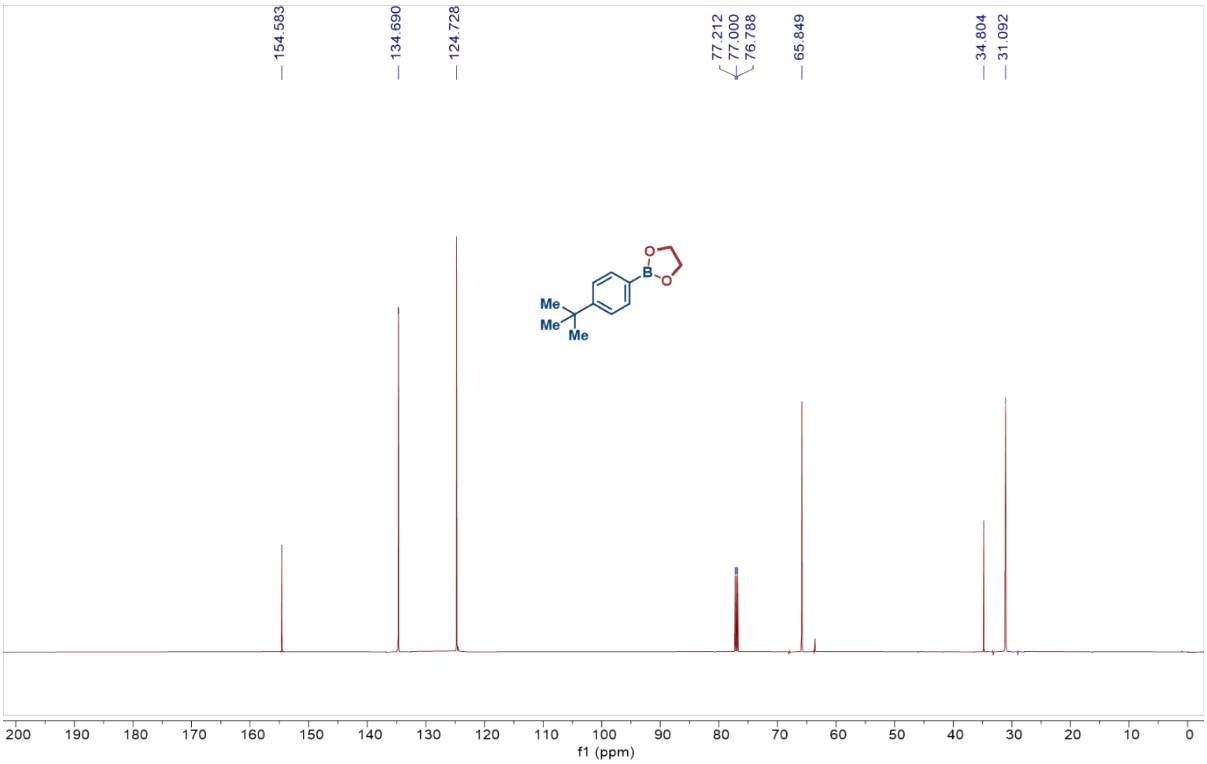

^{1}H NMR of **3e** (600 MHz, $CDCl_3$) and ^{13}C NMR of **3e** (151 MHz, $CDCl_3$)

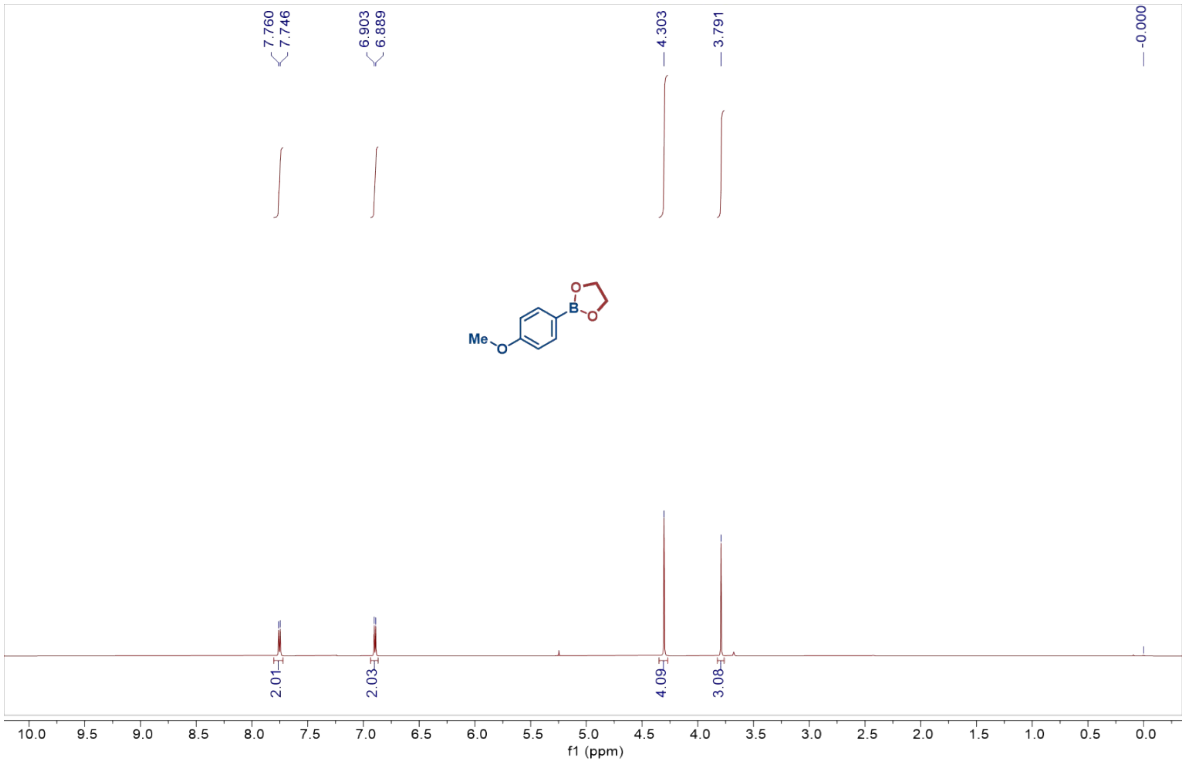

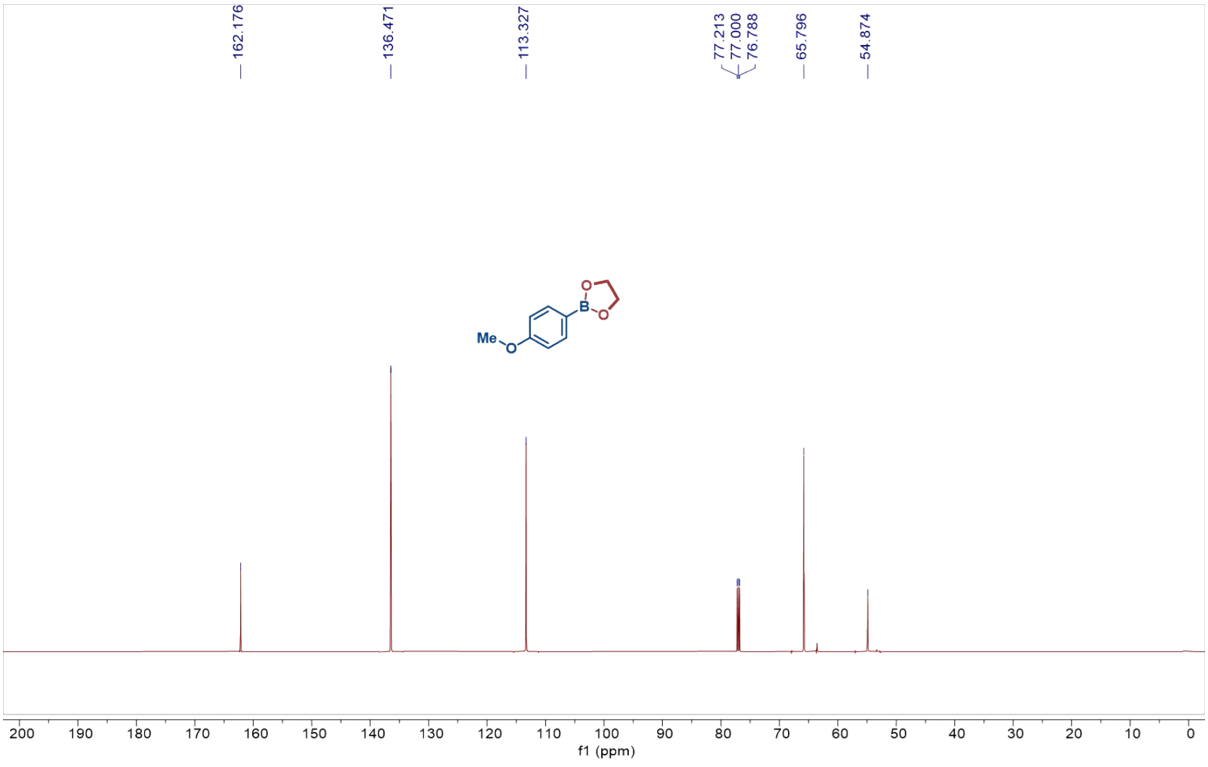

^{1}H NMR of **3f** (600 MHz, $CDCl_3$) and ^{13}C NMR of **3f** (151 MHz, $CDCl_3$)

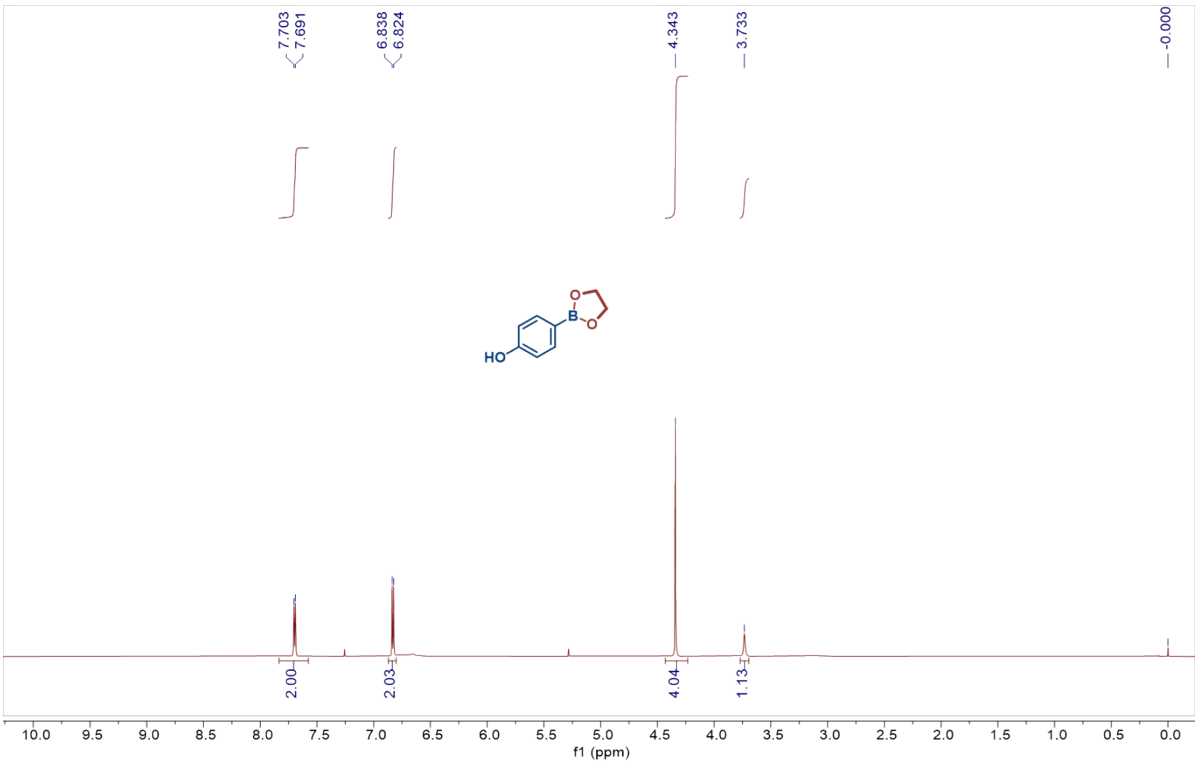

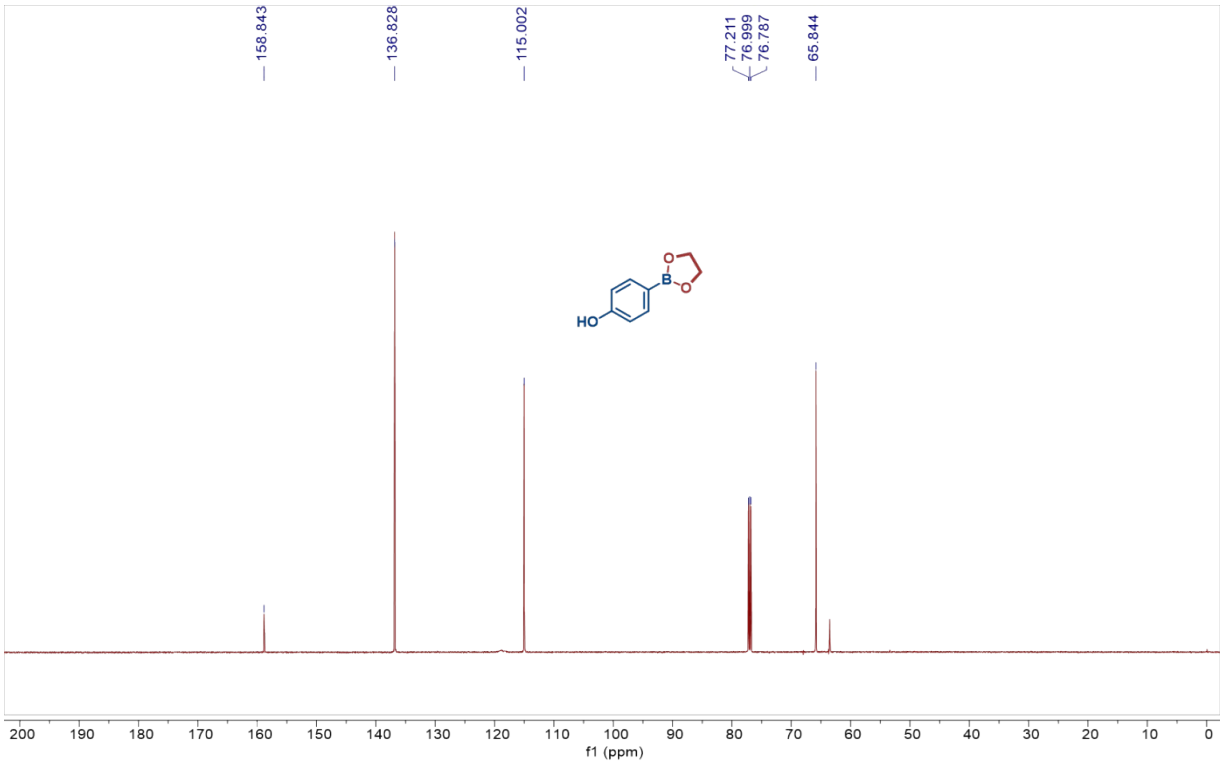

^{1}H NMR of **3g** (600 MHz, $CDCl_3$) and ^{13}C NMR of **3g** (151 MHz, $CDCl_3$)

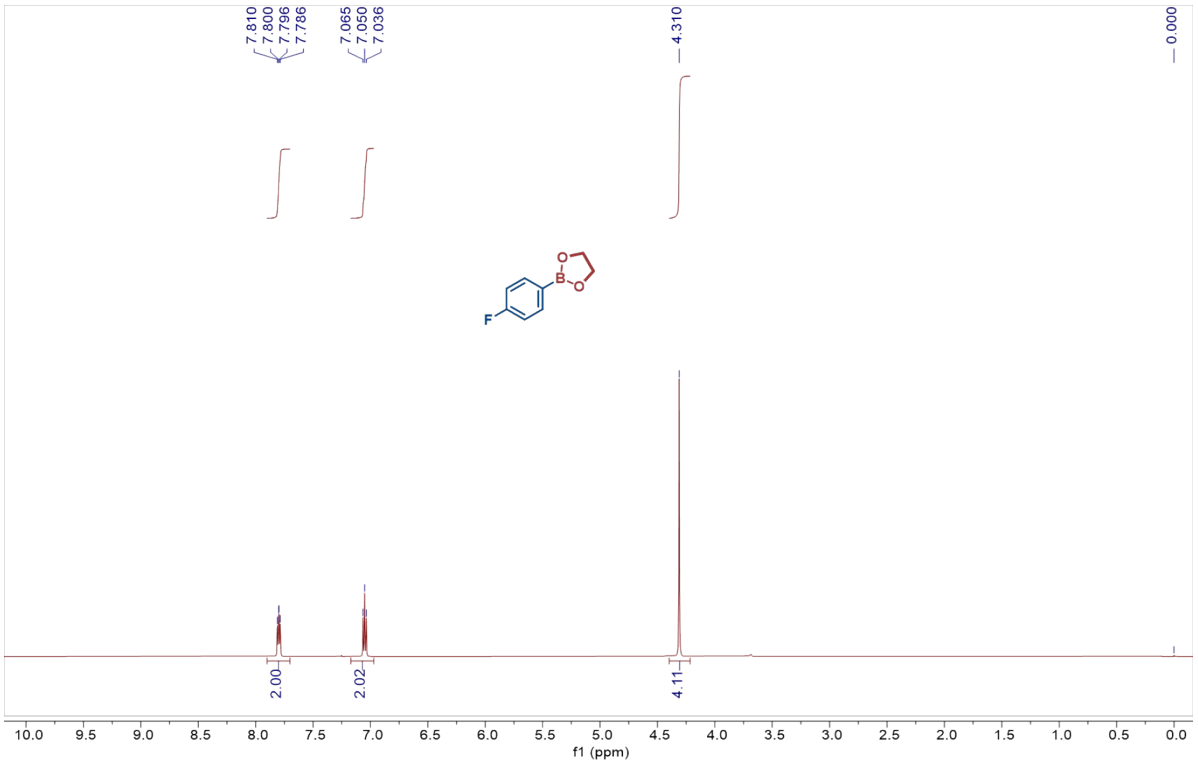

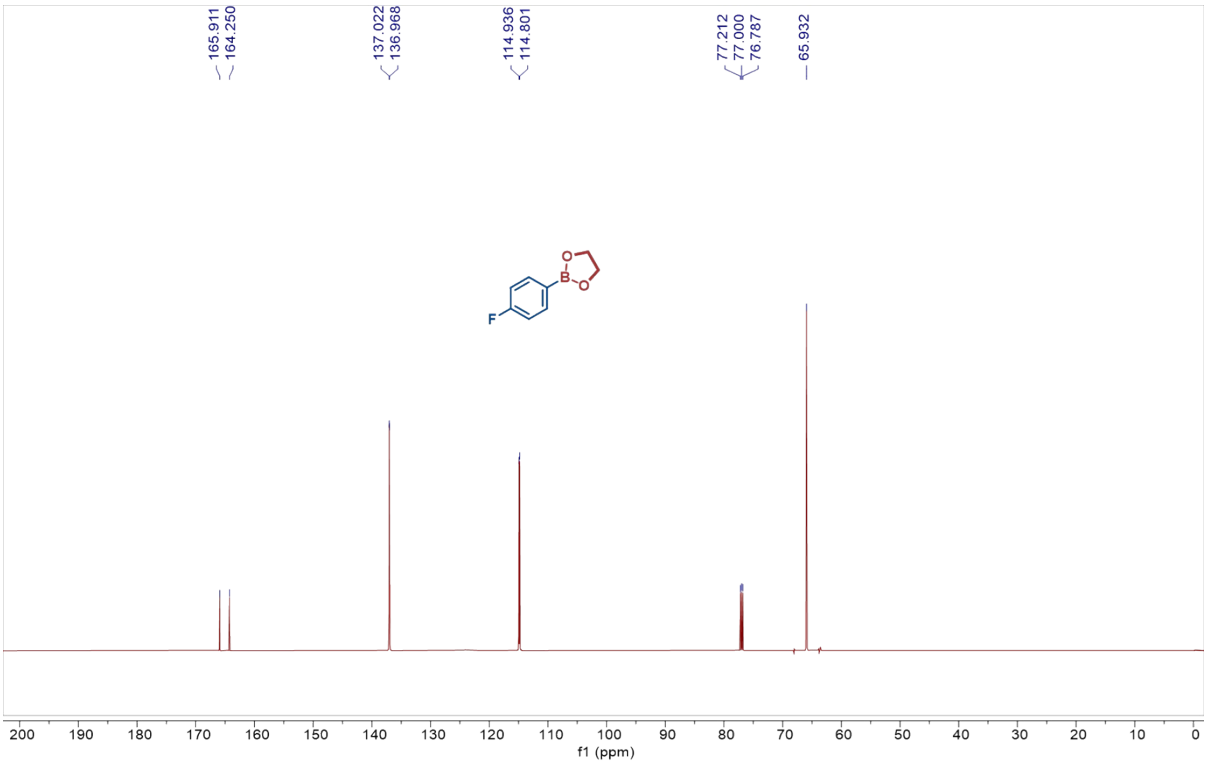

^{1}H NMR of **3h** (600 MHz, $CDCl_3$) and ^{13}C NMR of **3h** (151 MHz, $CDCl_3$)

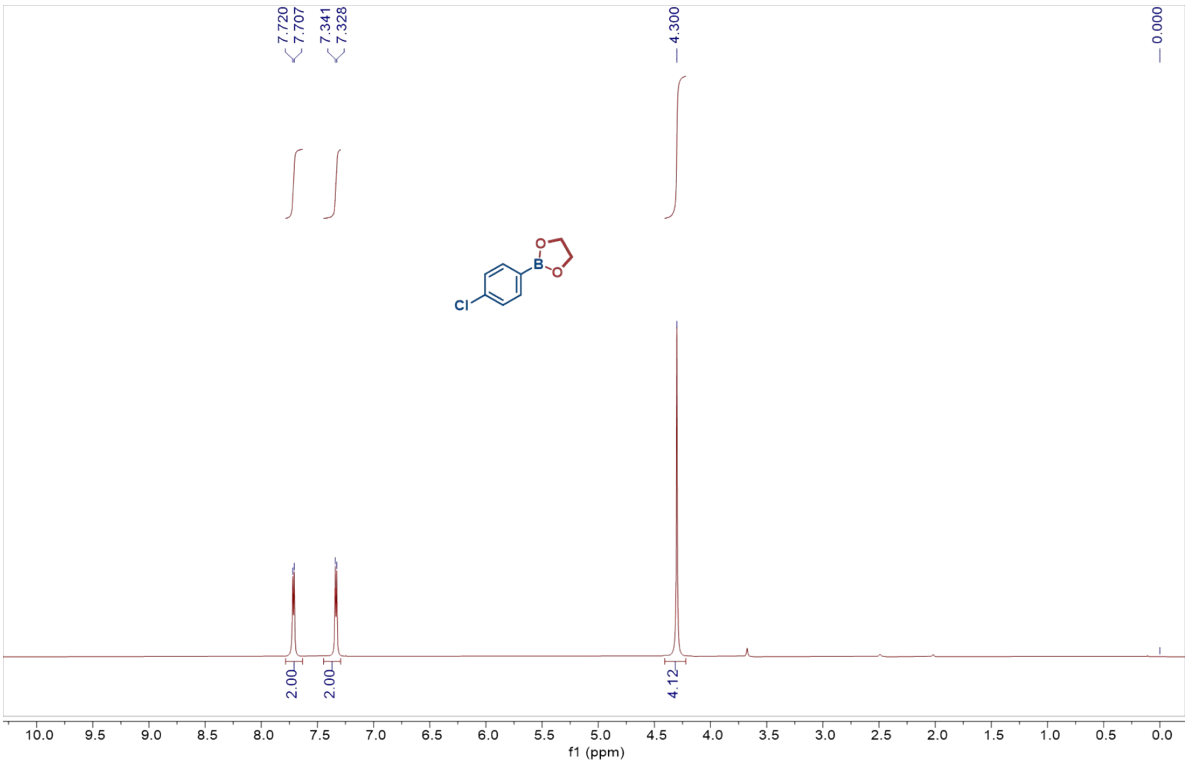

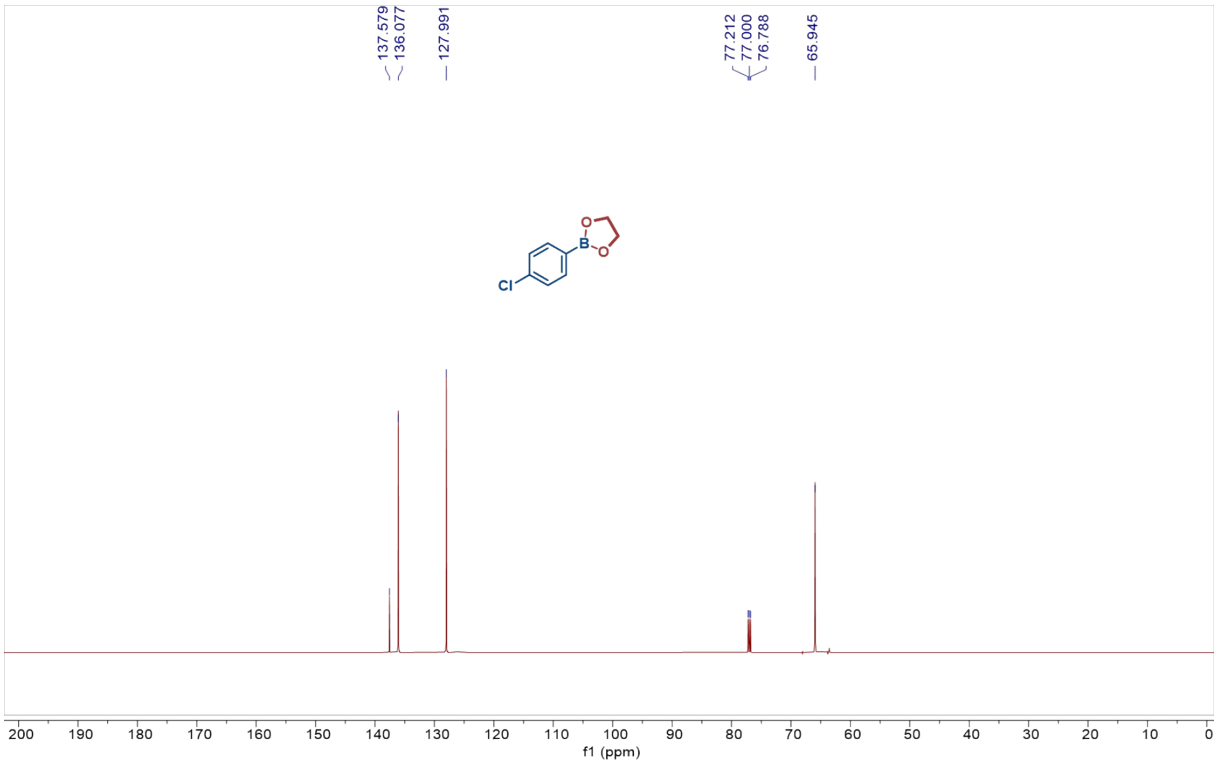

^{1}H NMR of **3i** (600 MHz, $CDCl_3$) and ^{13}C NMR of **3i** (151 MHz, $CDCl_3$)

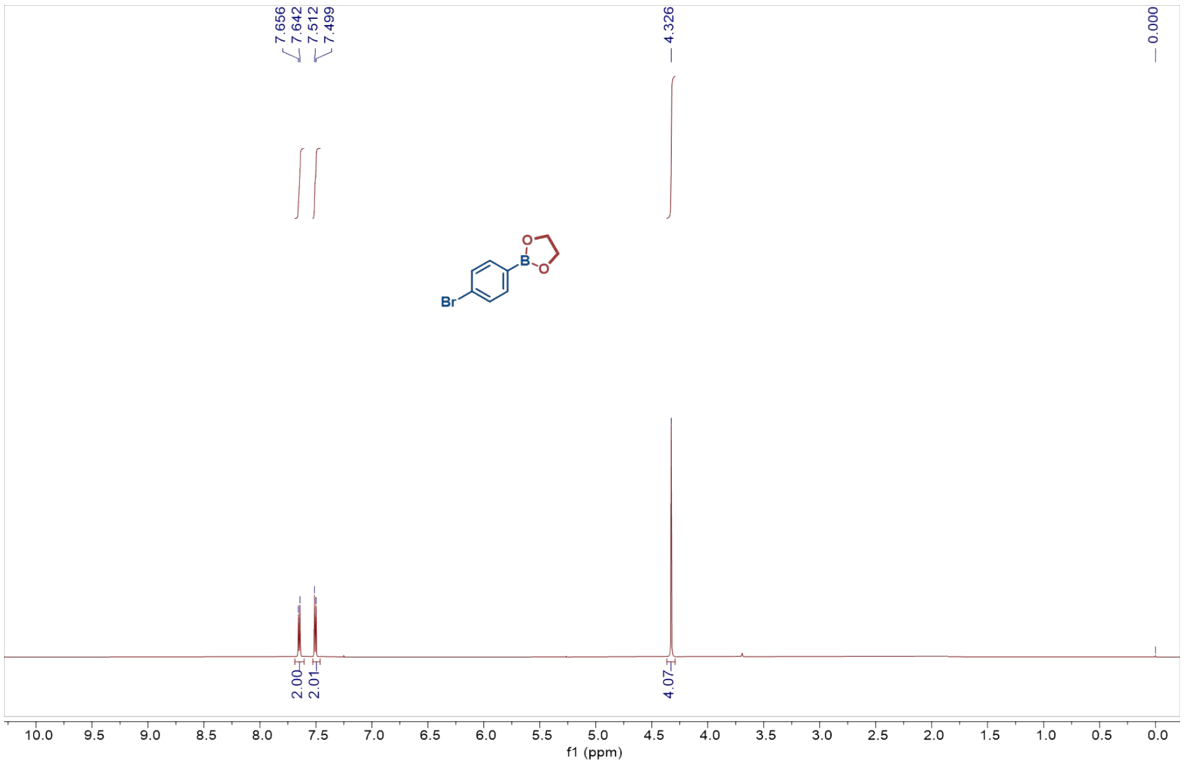

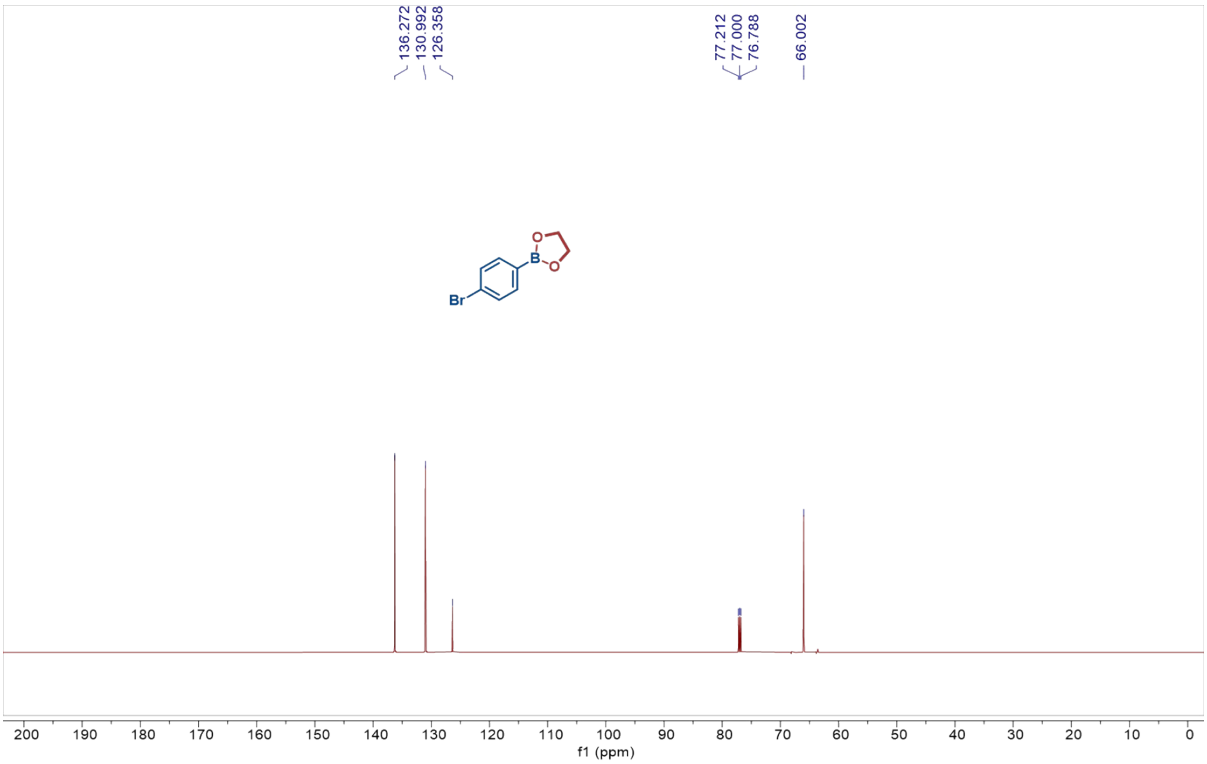

^{1}H NMR of **3j** (600 MHz, $CDCl_3$) and ^{13}C NMR of **3j** (151 MHz, $CDCl_3$)

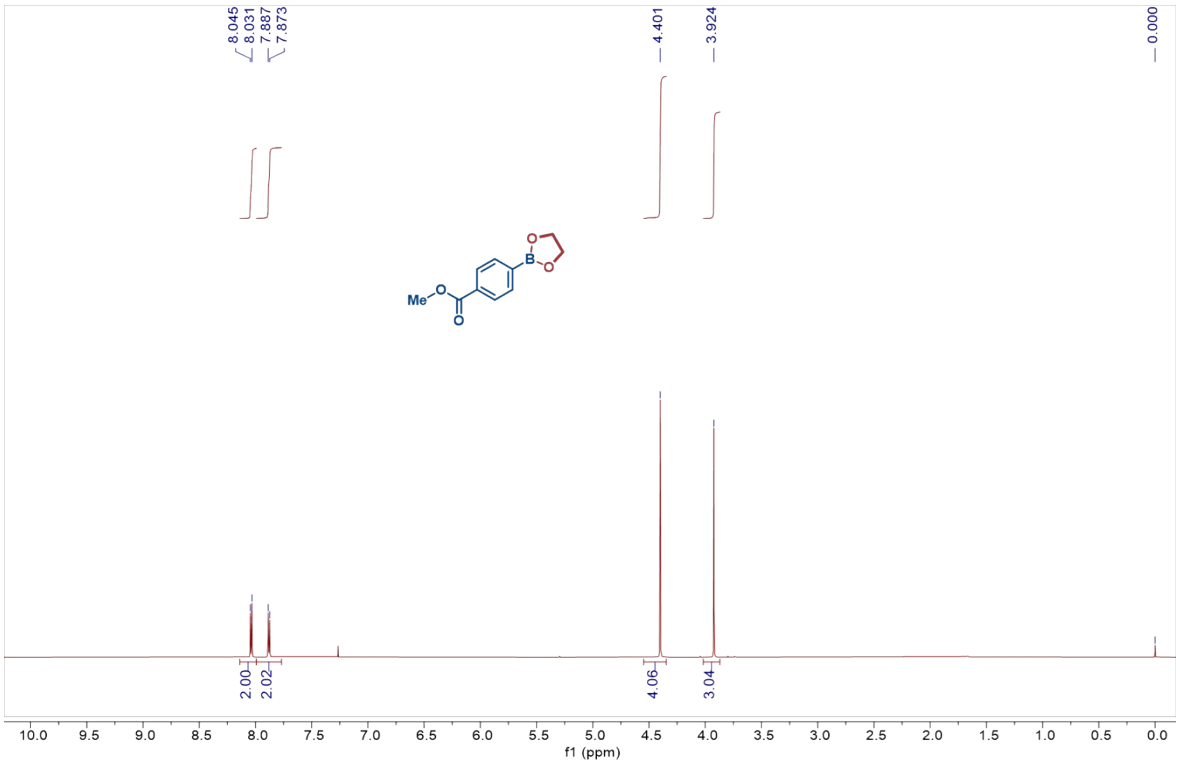

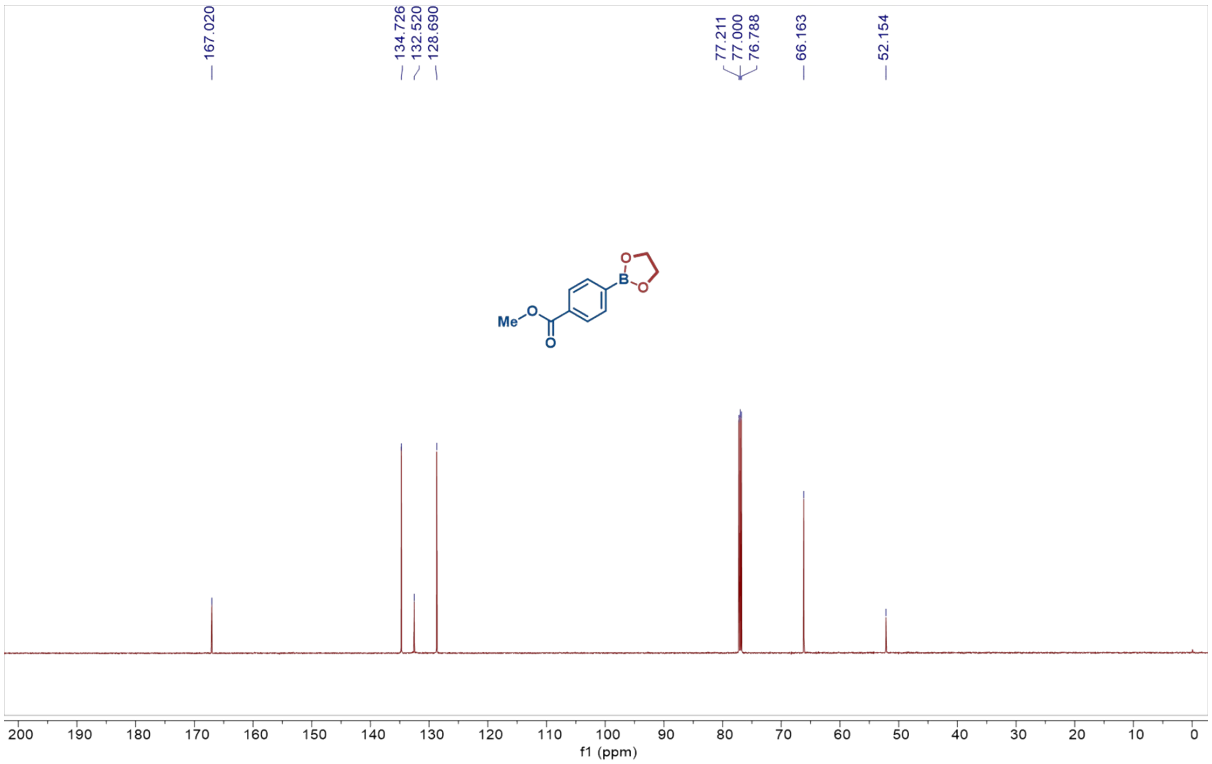

^{1}H NMR of **3k** (600 MHz, $CDCl_3$) and ^{13}C NMR of **3k** (151 MHz, $CDCl_3$)

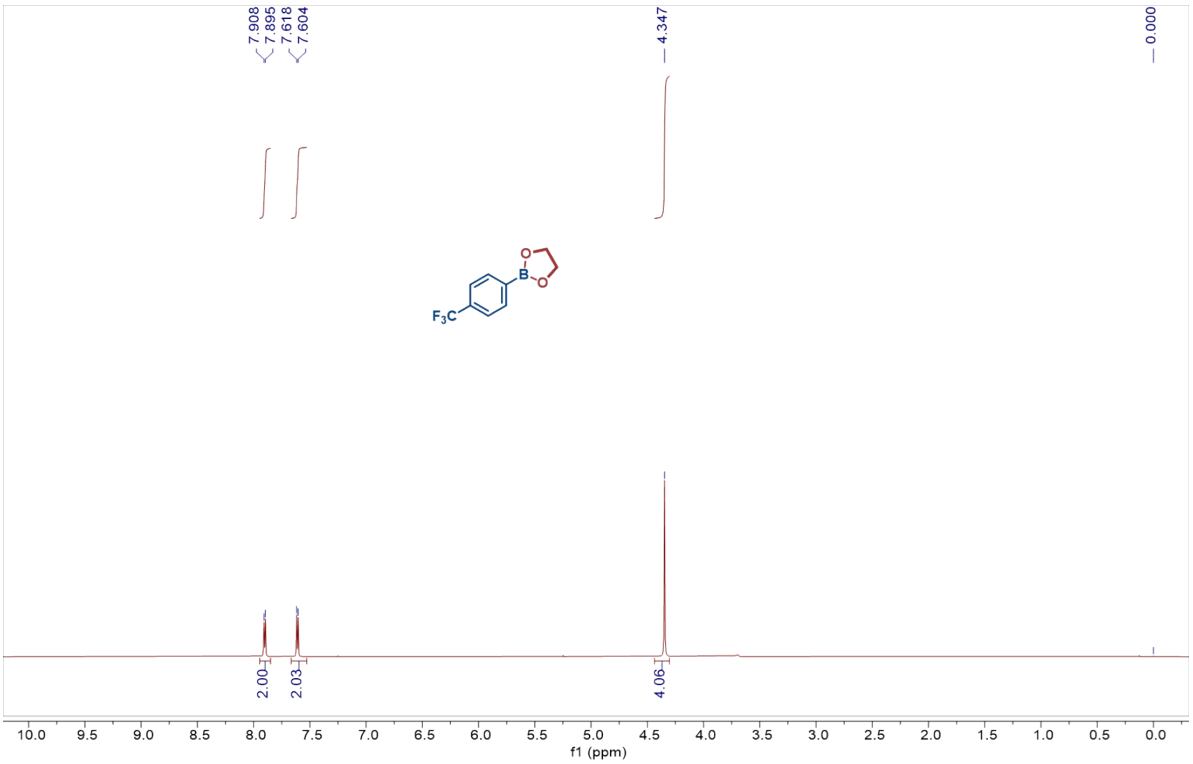

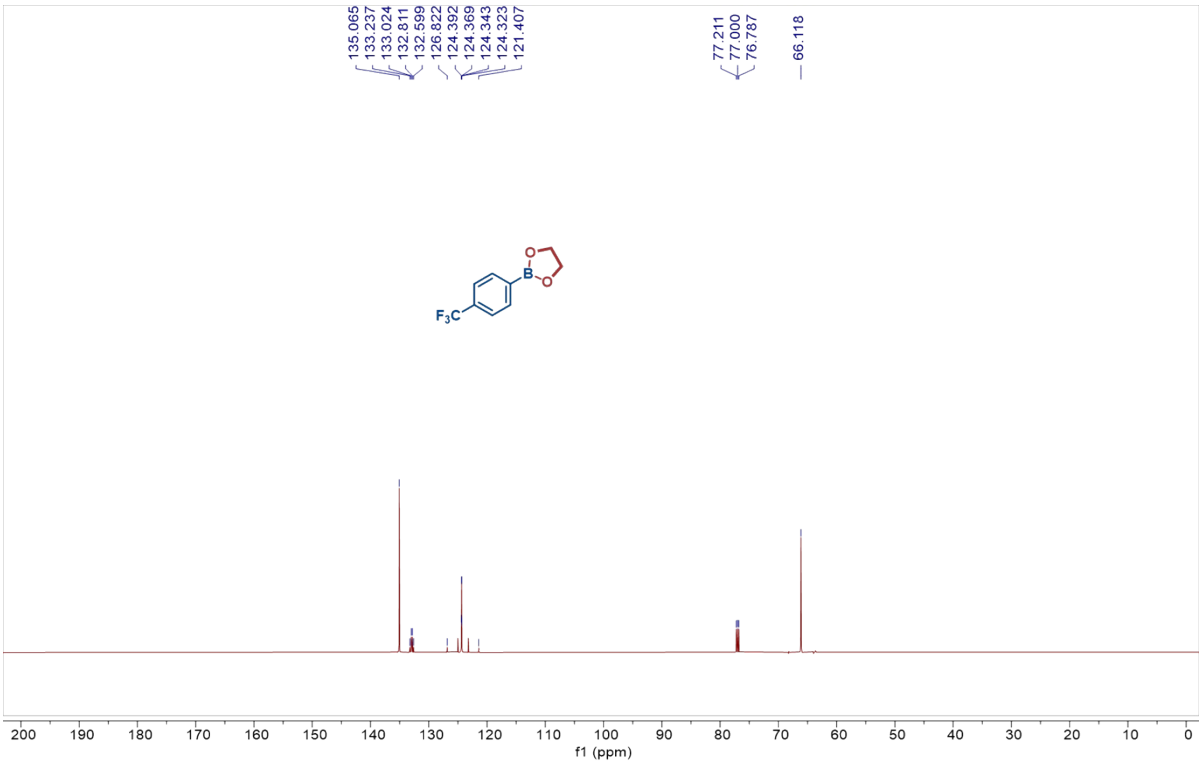

^{1}H NMR of **3l** (600 MHz, $CDCl_3$) and ^{13}C NMR of **3l** (151 MHz, $CDCl_3$)

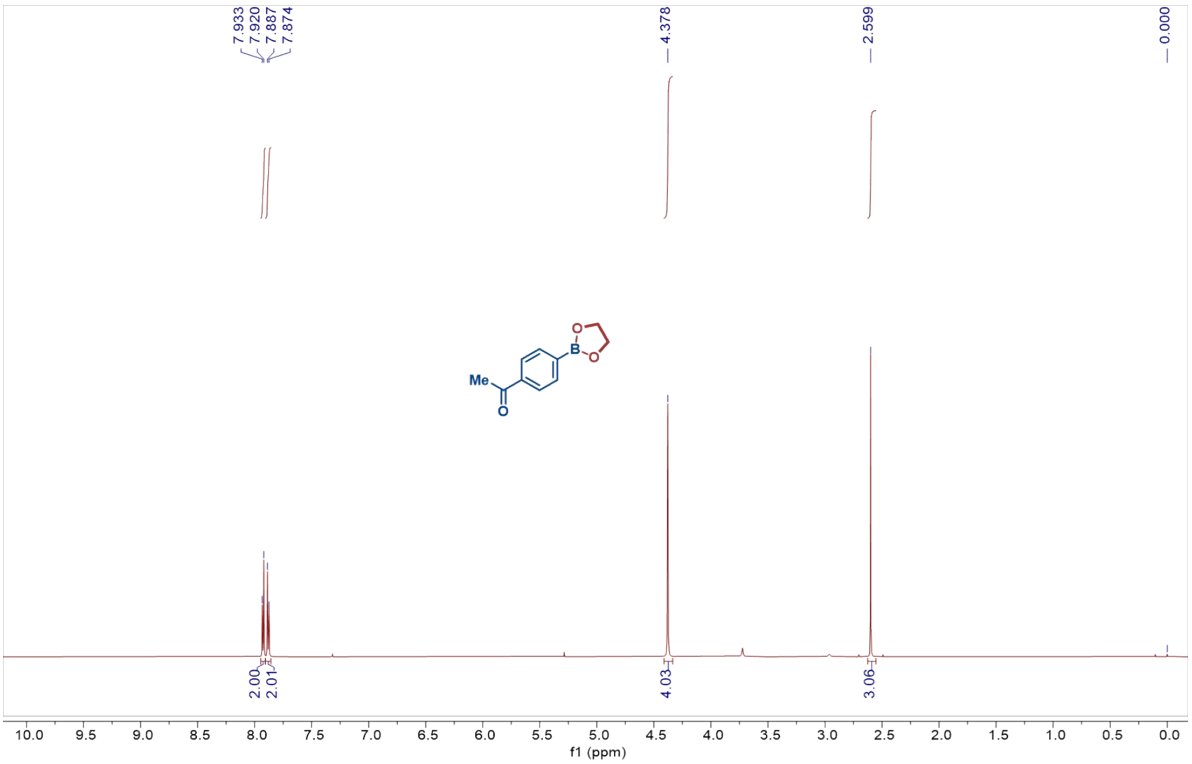

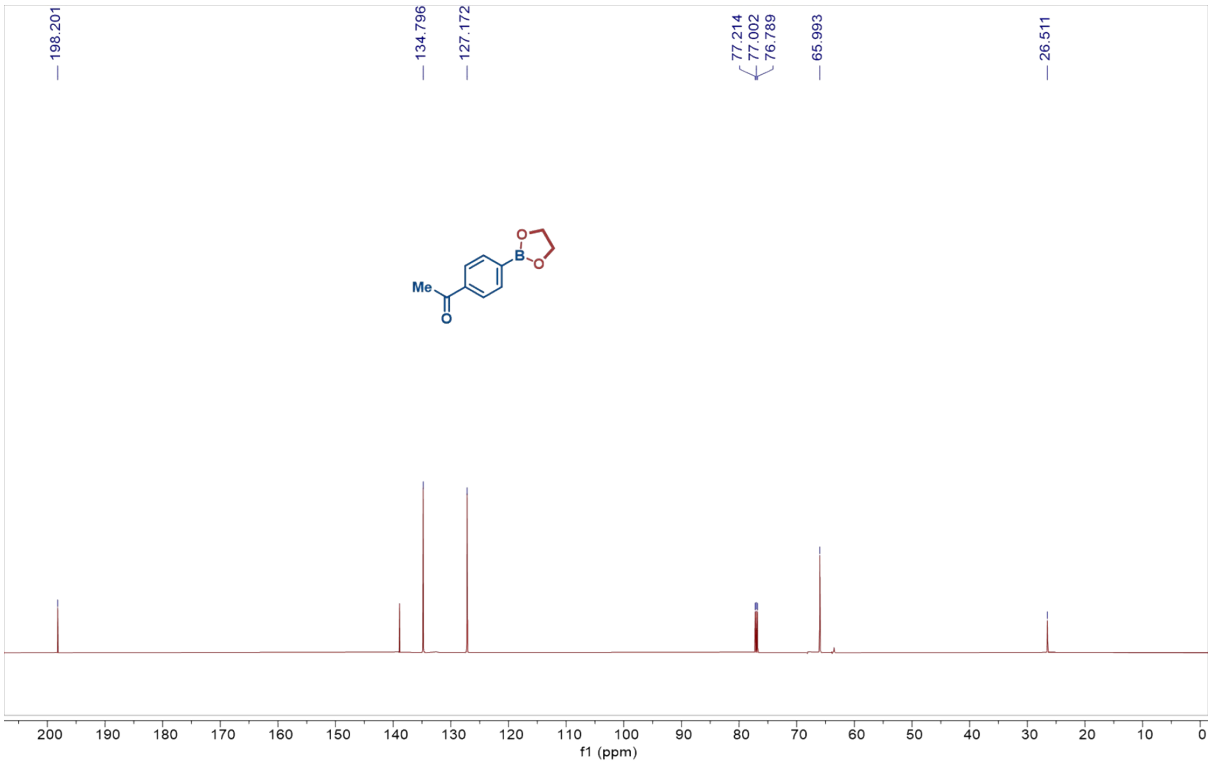

^{1}H NMR of **3m** (600 MHz, $CDCl_3$) and ^{13}C NMR of **3m** (151 MHz, $CDCl_3$)

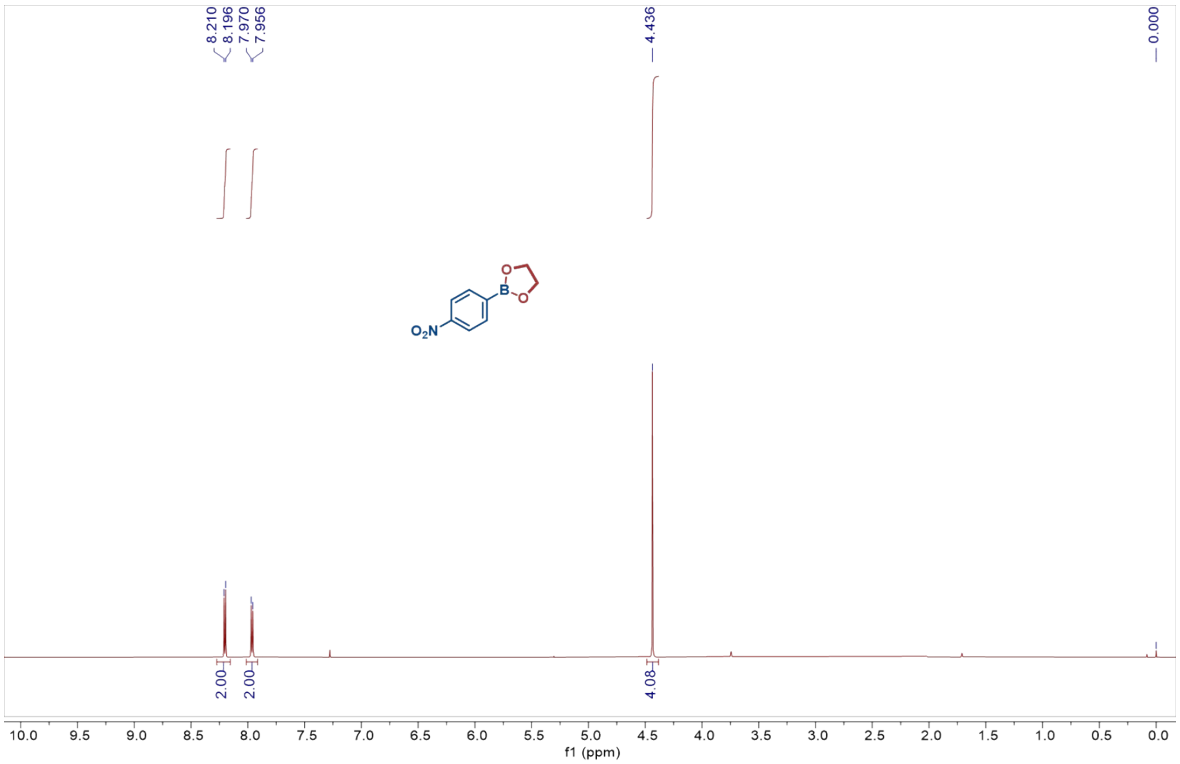

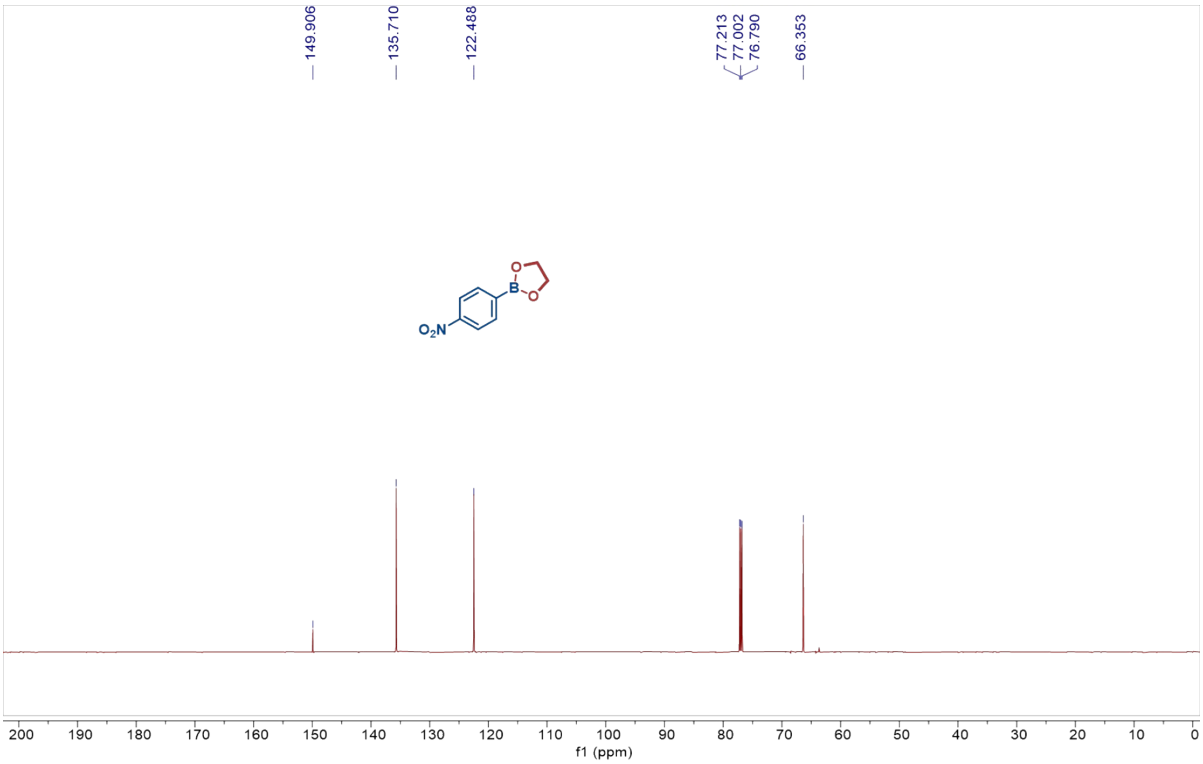

^{1}H NMR of **3n** (600 MHz, $CDCl_3$) and ^{13}C NMR of **3n** (151 MHz, $CDCl_3$)

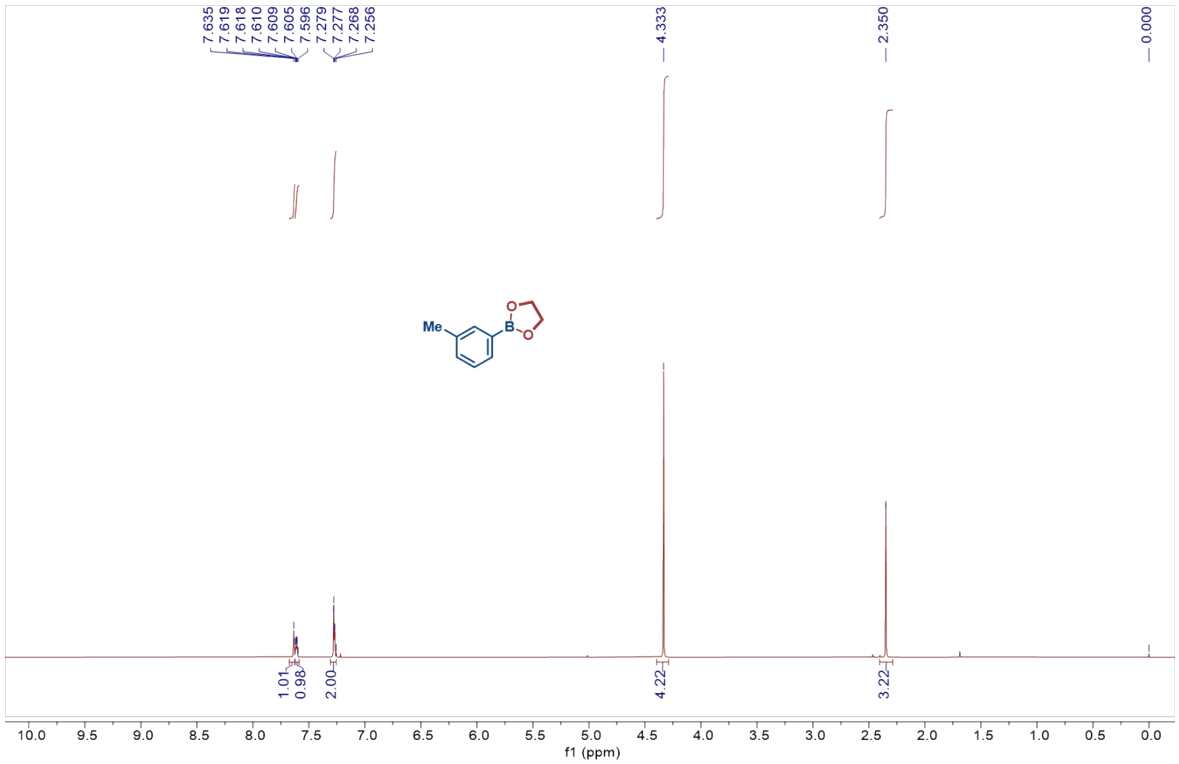

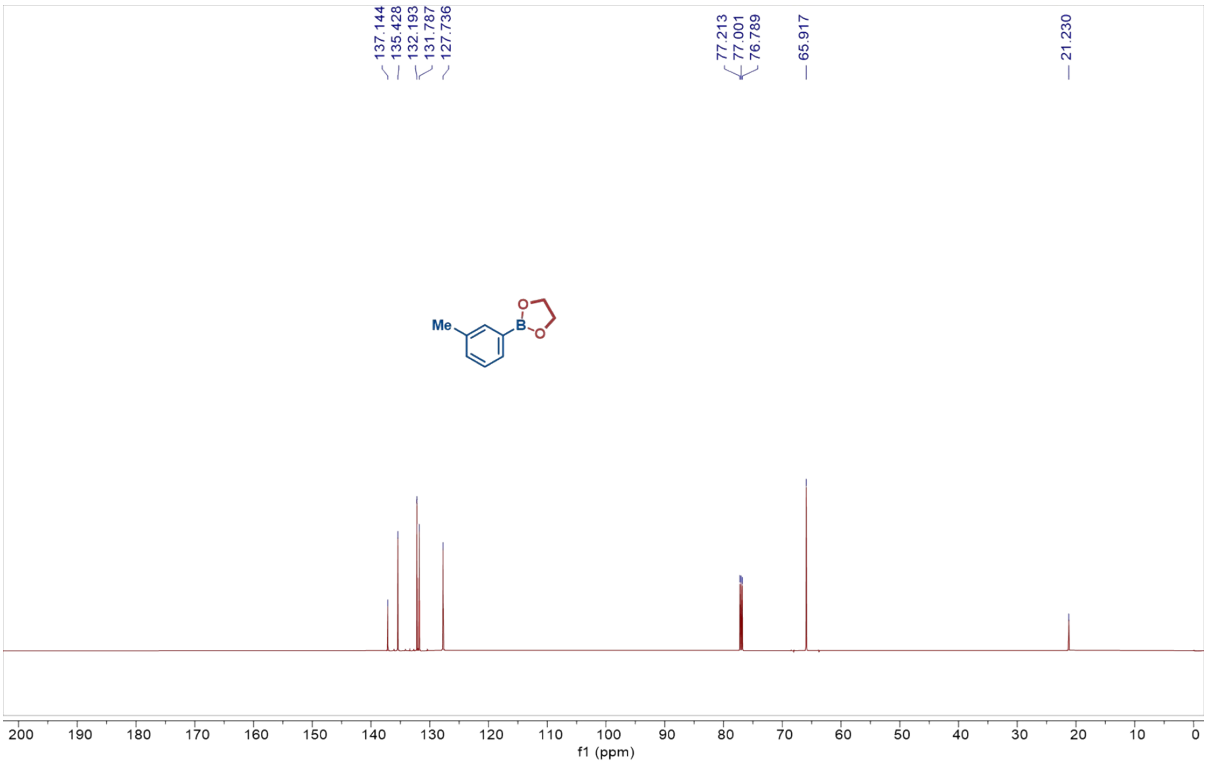

^{1}H NMR of **3o** (600 MHz, $CDCl_3$) and ^{13}C NMR of **3o** (151 MHz, $CDCl_3$)

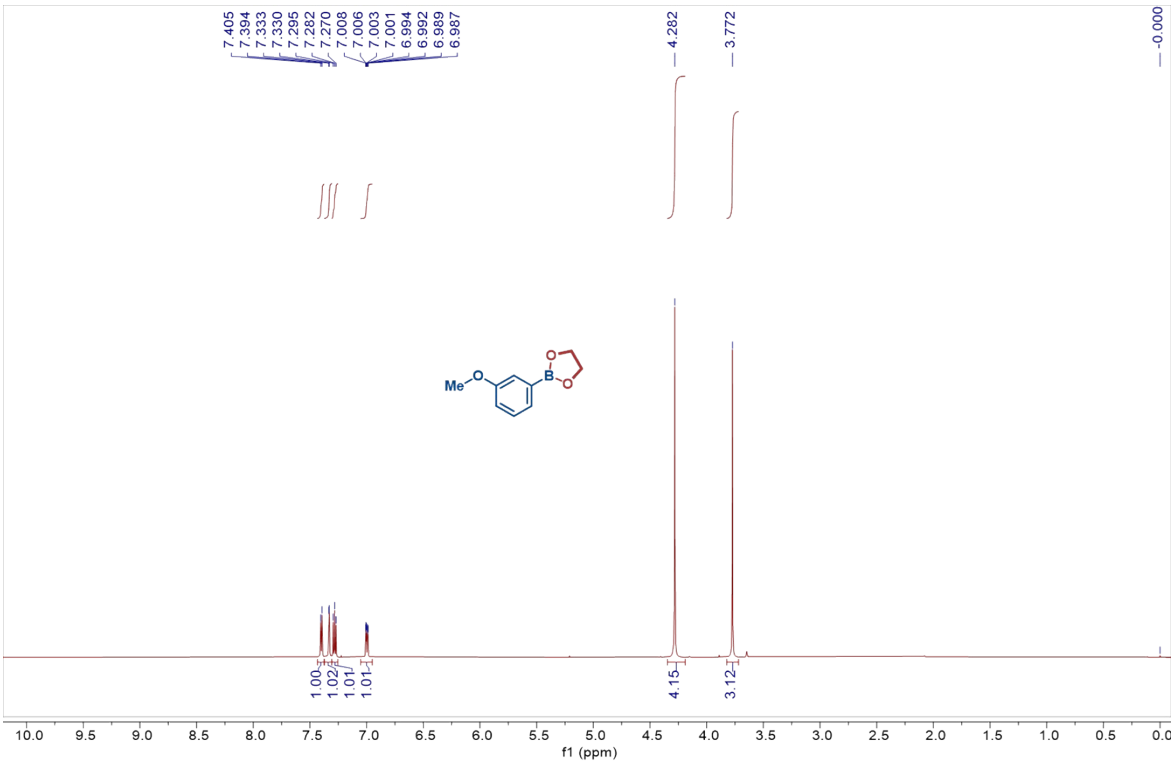

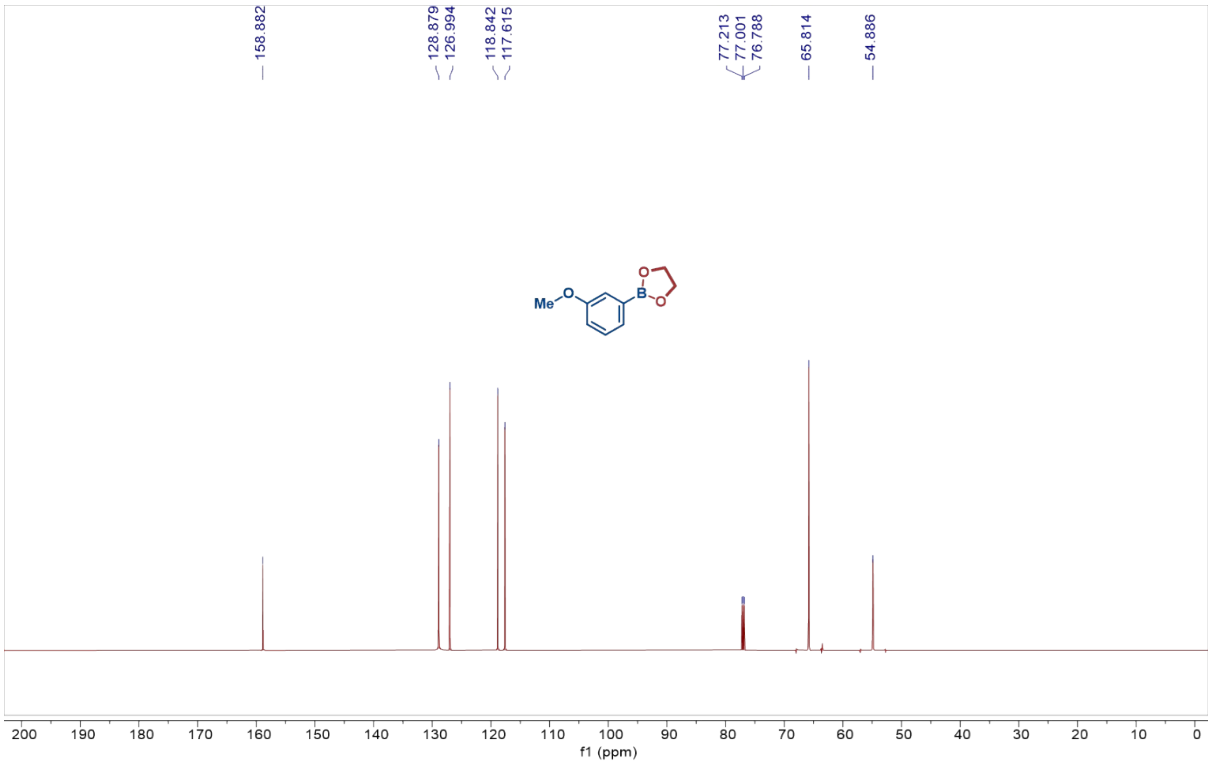

^{1}H NMR of **3p** (600 MHz, $CDCl_3$) and ^{13}C NMR of **3p** (151 MHz, $CDCl_3$)

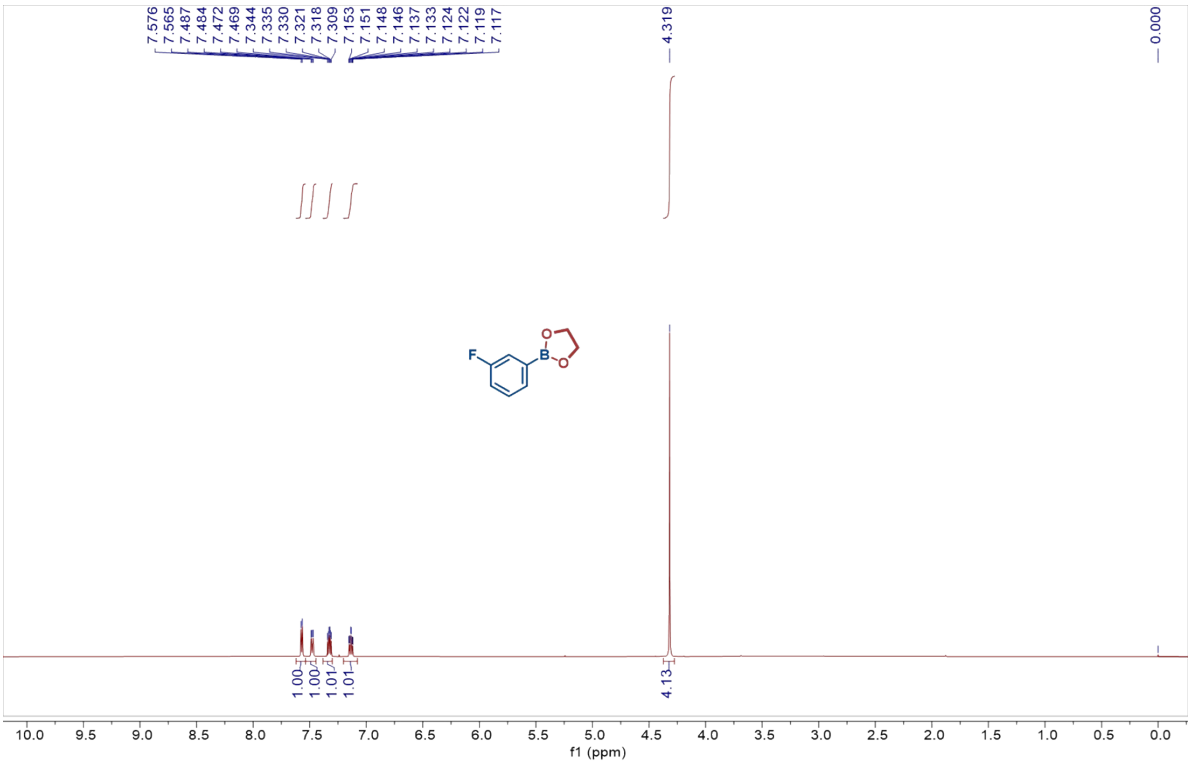

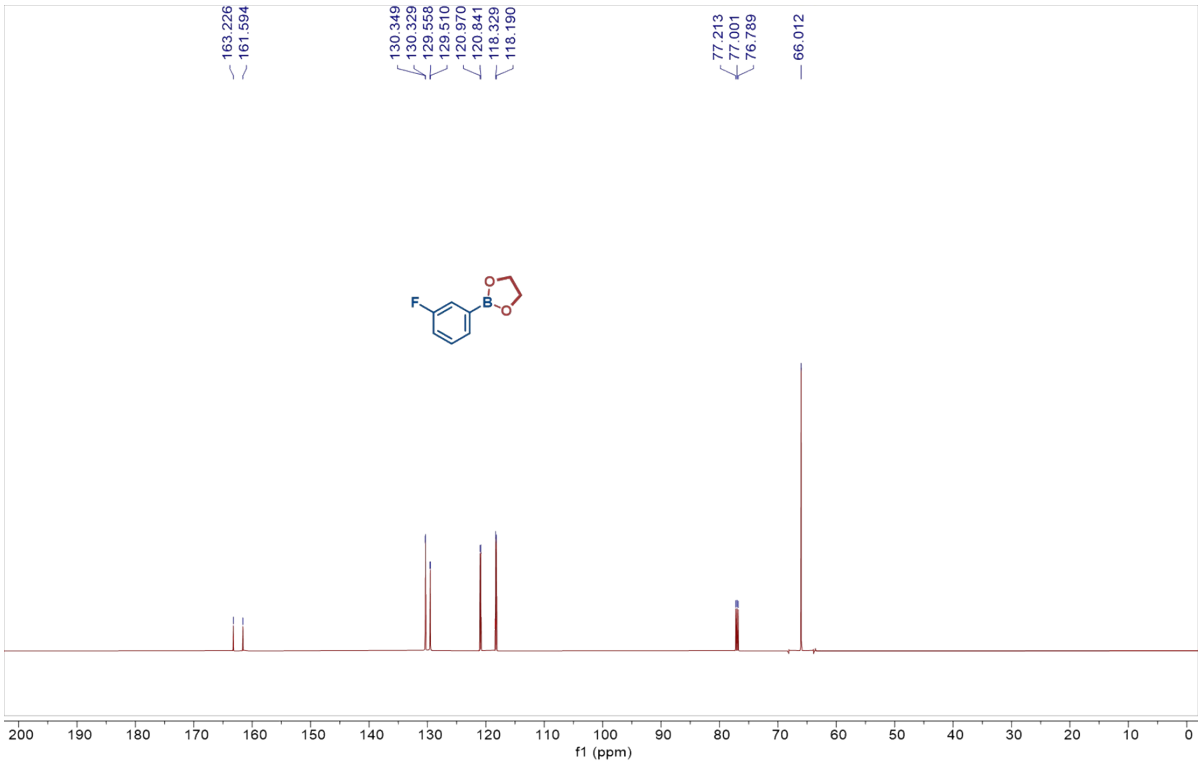

^{1}H NMR of **3q** (600 MHz, $CDCl_3$) and ^{13}C NMR of **3q** (151 MHz, $CDCl_3$)

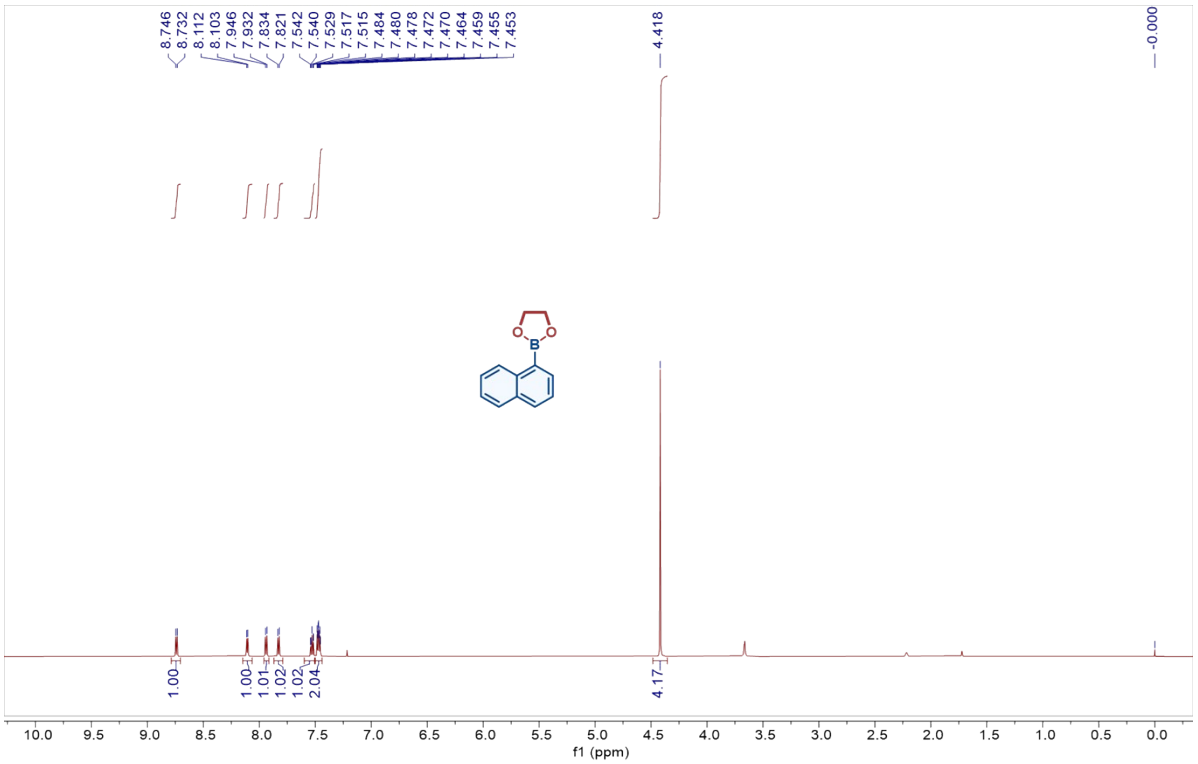

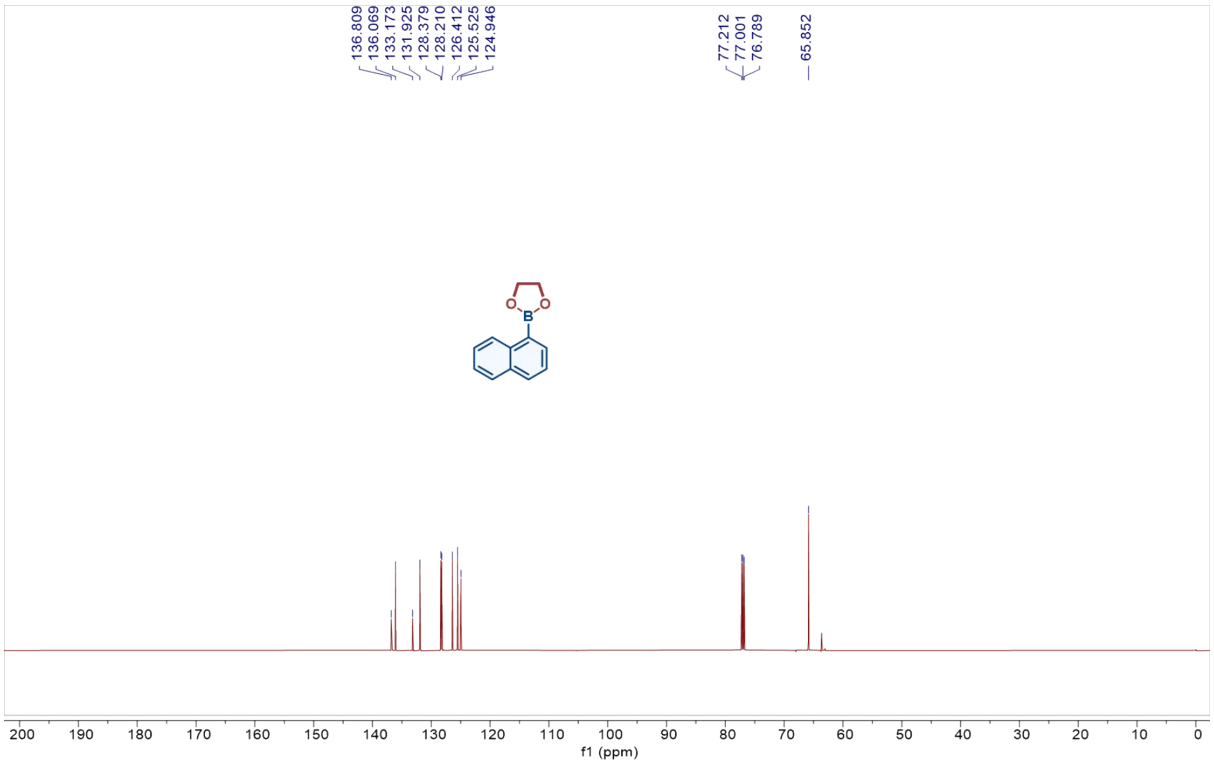

^{1}H NMR of **3r** (600 MHz, $CDCl_3$) and ^{13}C NMR of **3r** (151 MHz, $CDCl_3$)

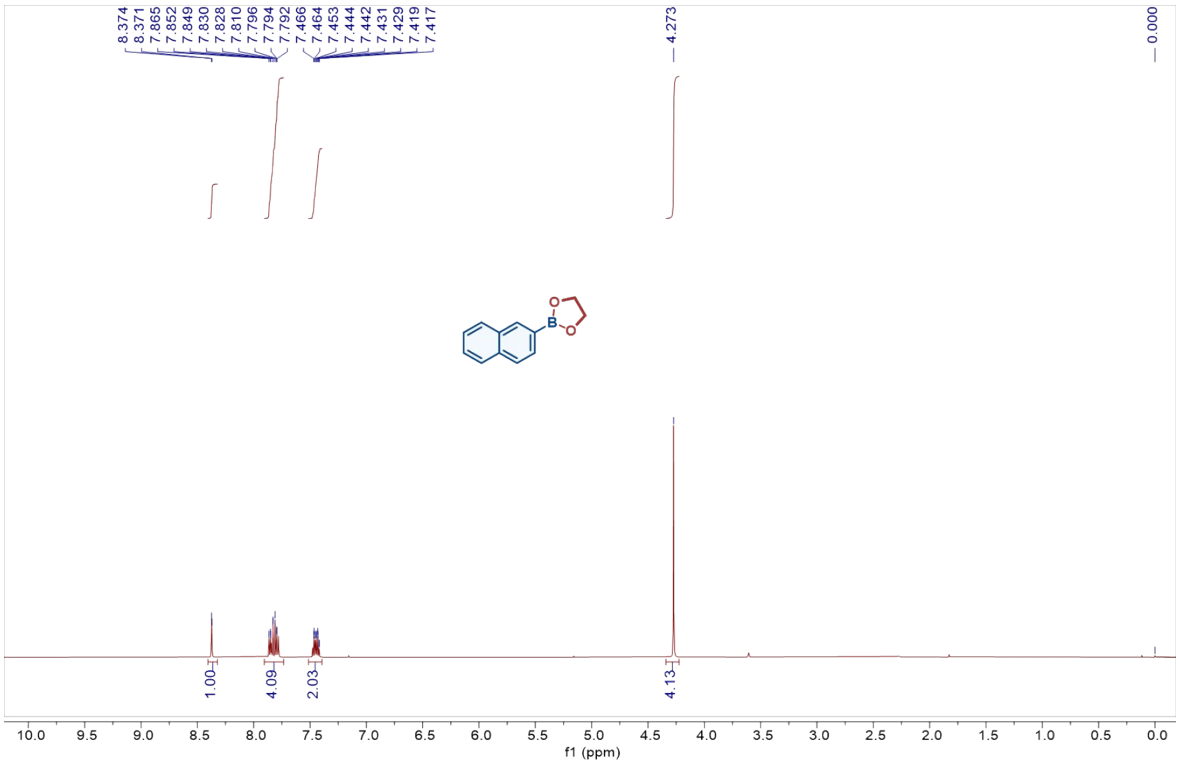

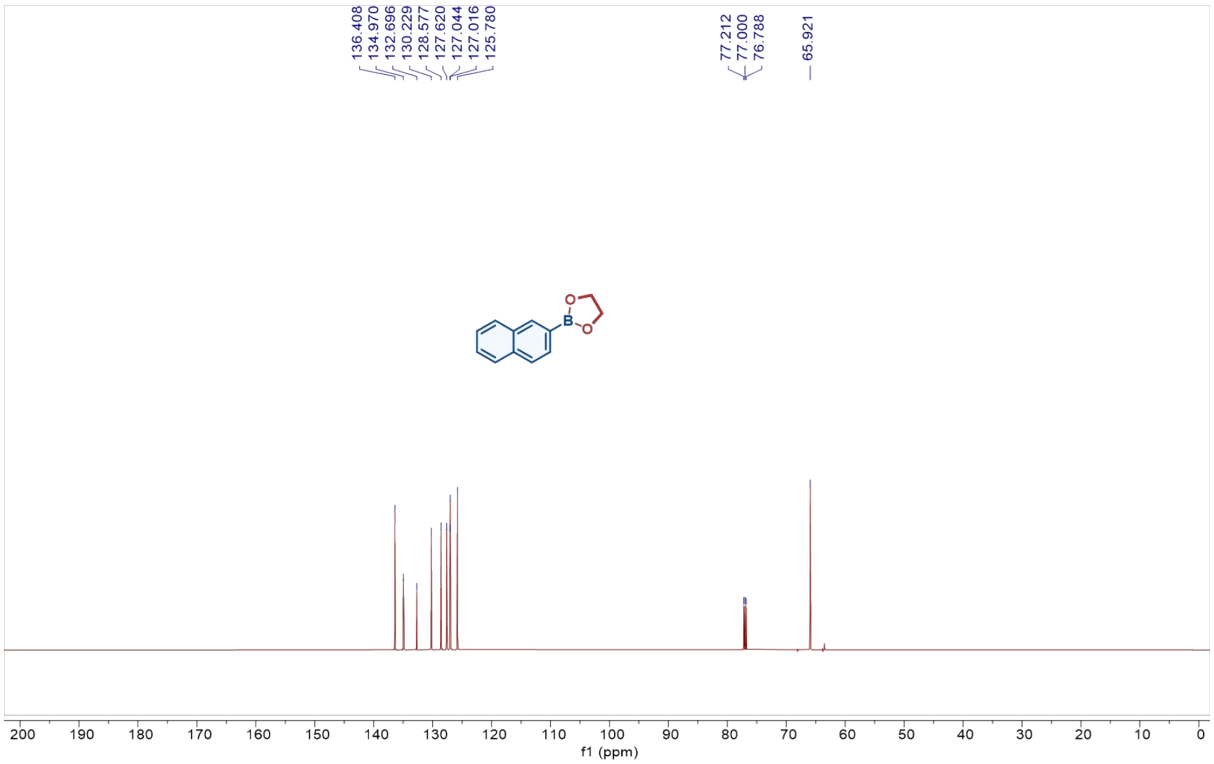

^{1}H NMR of **3s** (600 MHz, $CDCl_3$) and ^{13}C NMR of **3s** (151 MHz, $CDCl_3$)

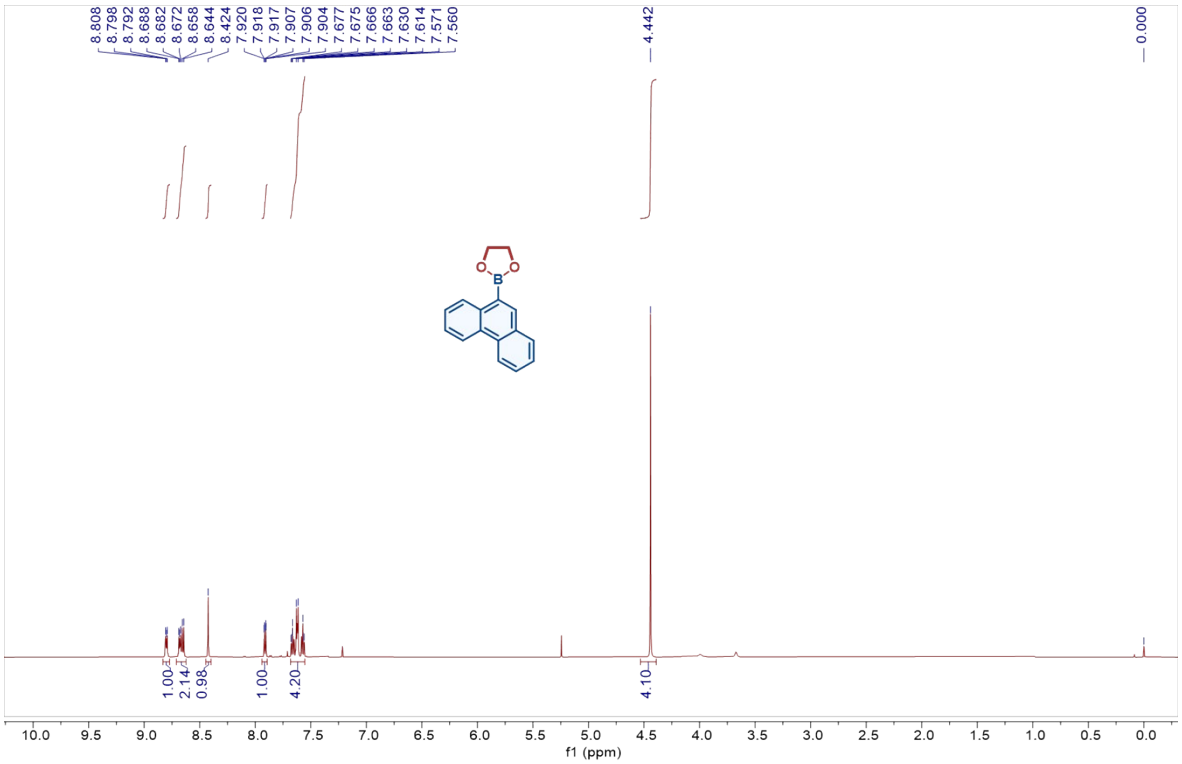

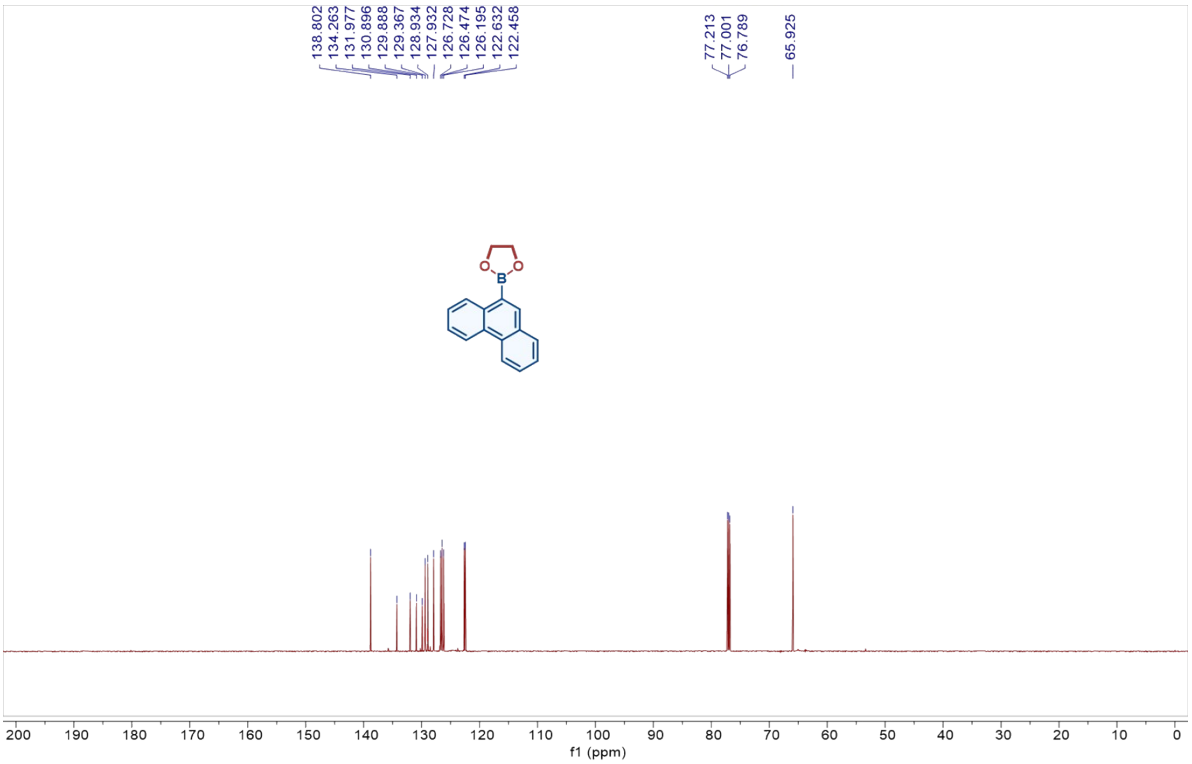

^{1}H NMR of **3t** (600 MHz, $CDCl_3$) and ^{13}C NMR of **3t** (151 MHz, $CDCl_3$)

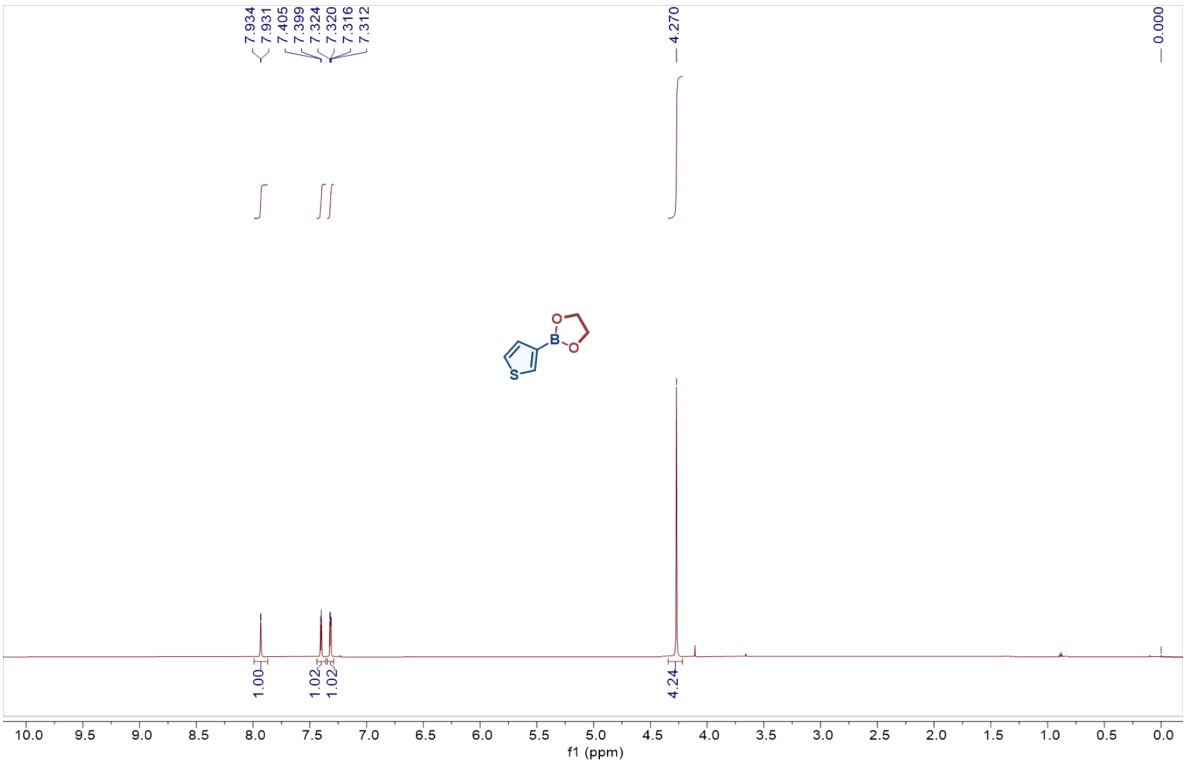

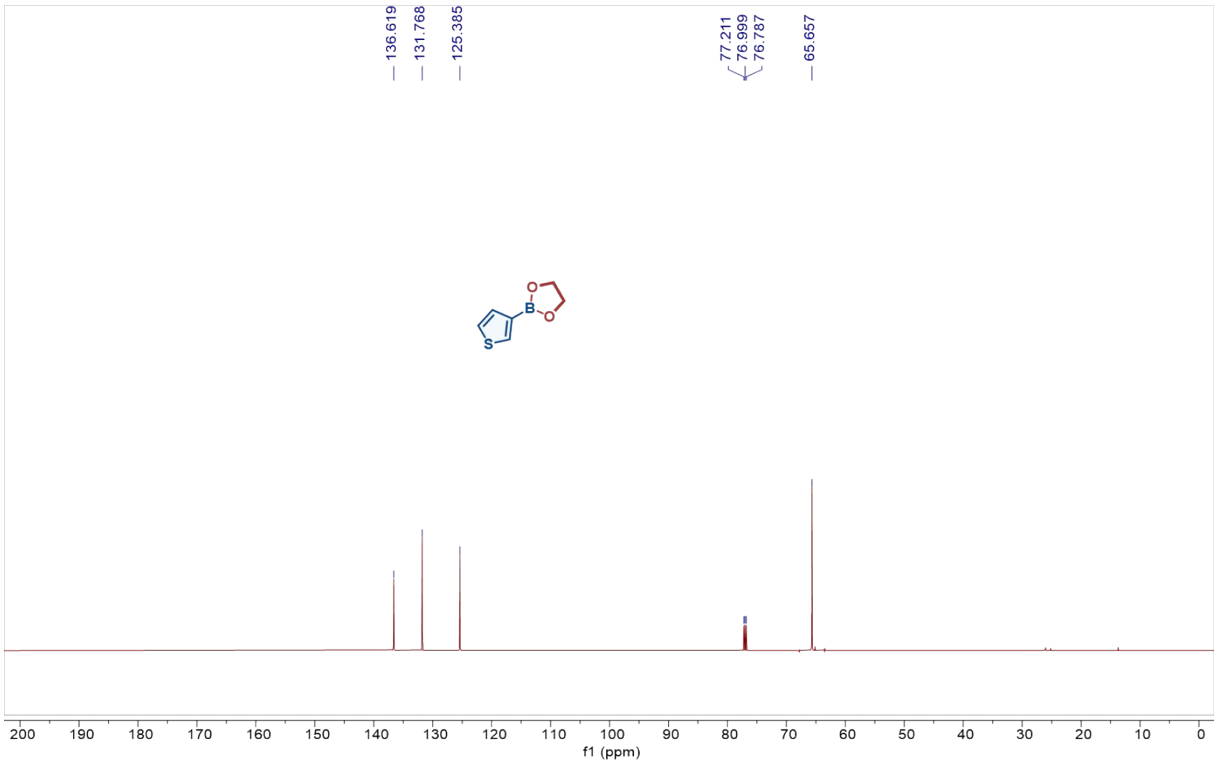

^{1}H NMR of **3u** (600 MHz, $CDCl_3$) and ^{13}C NMR of **3u** (151 MHz, $CDCl_3$)

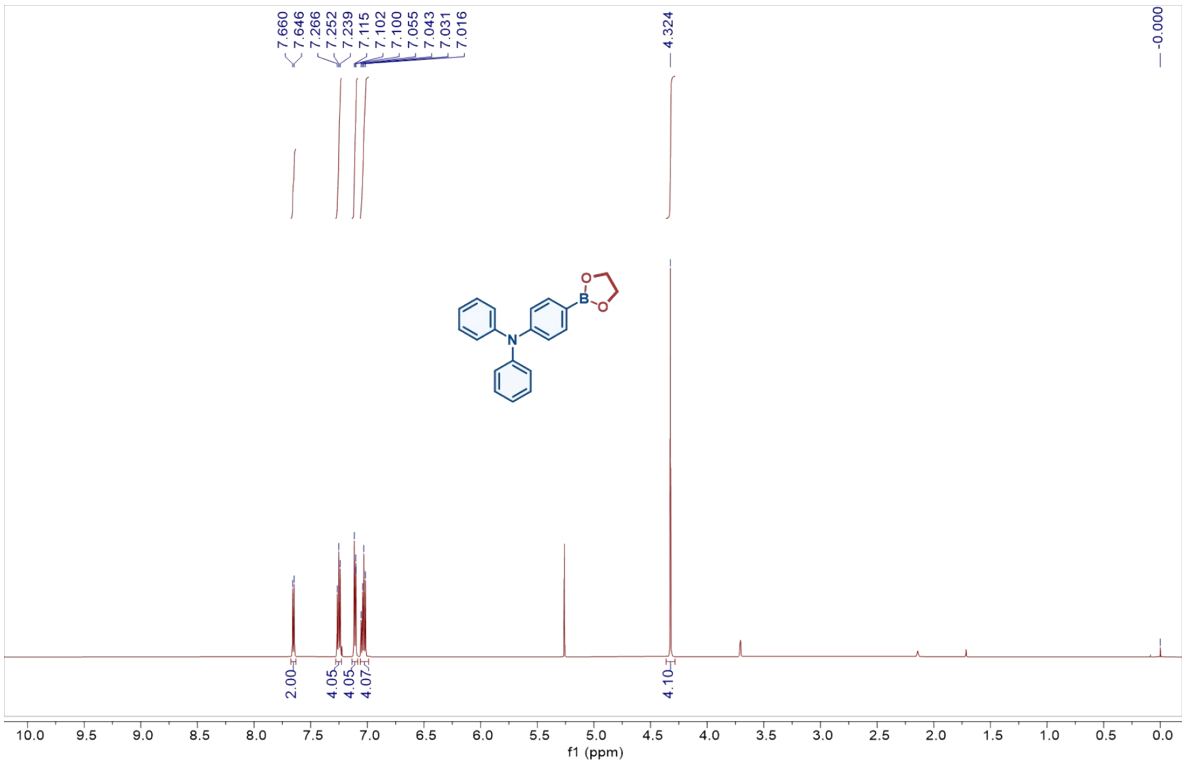

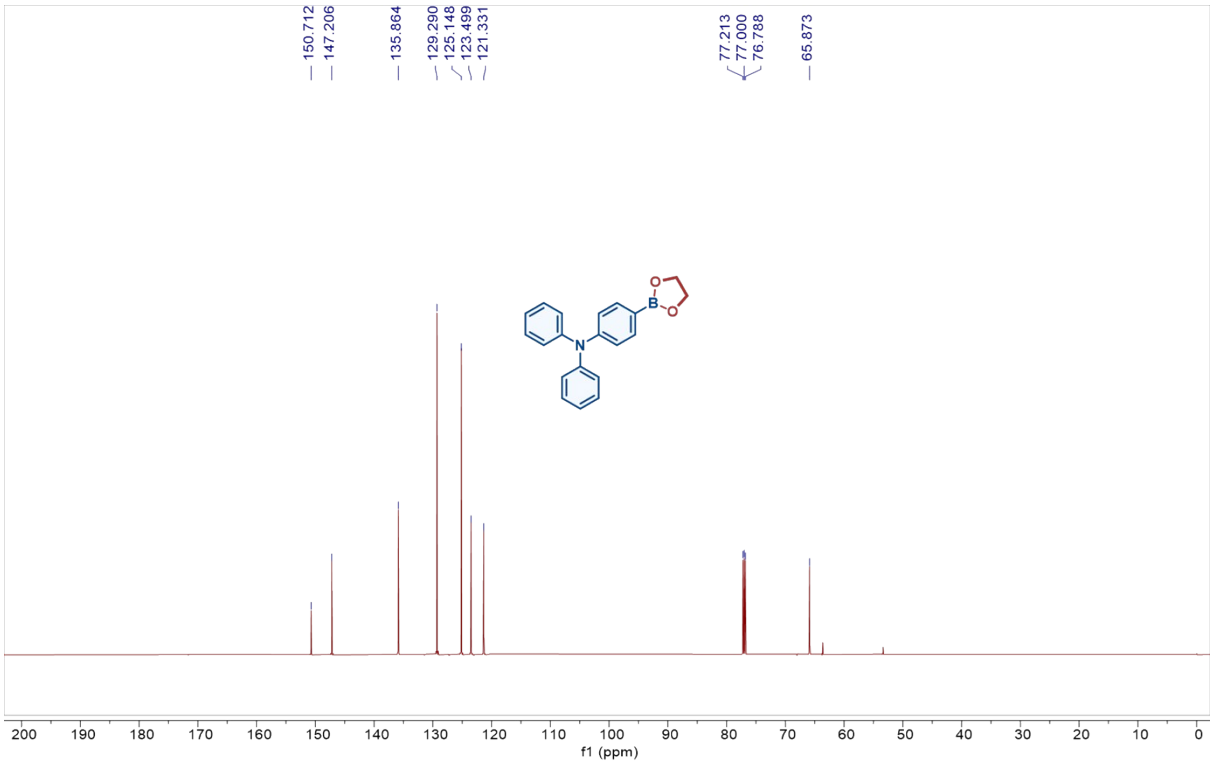

^{1}H NMR of **3v** (600 MHz, $CDCl_3$) and ^{13}C NMR of **3v** (151 MHz, $CDCl_3$)

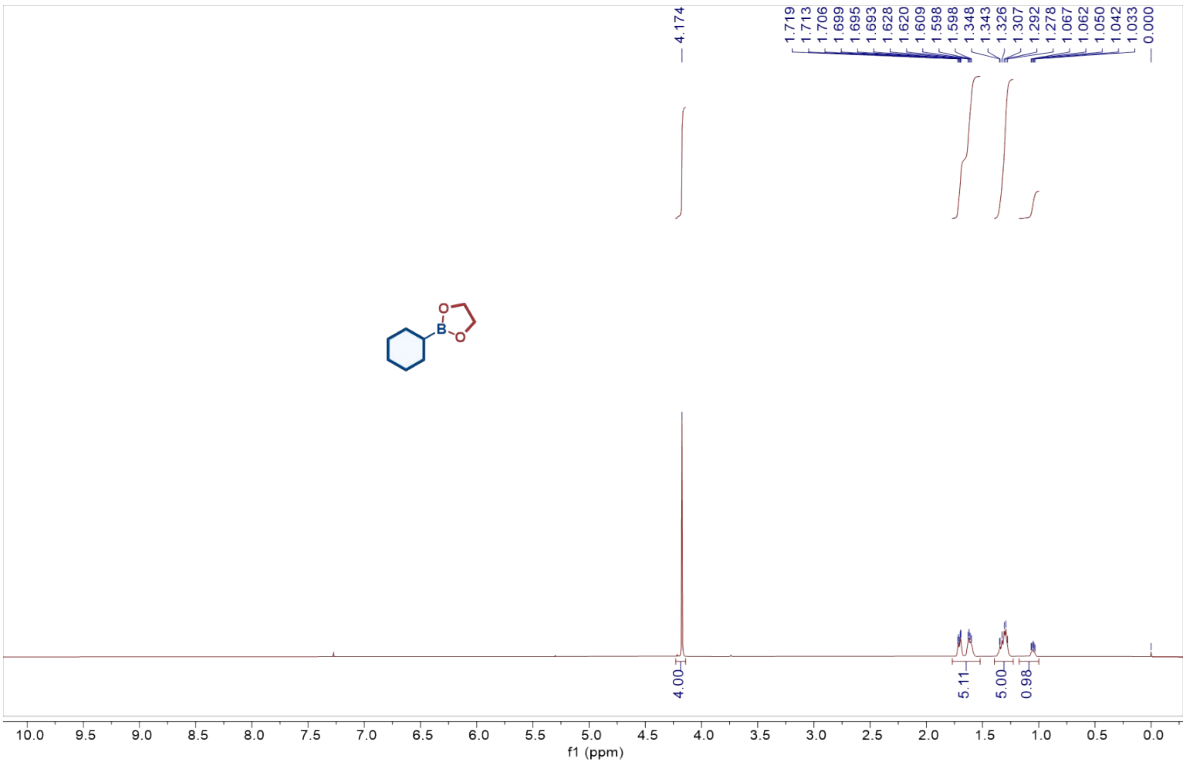

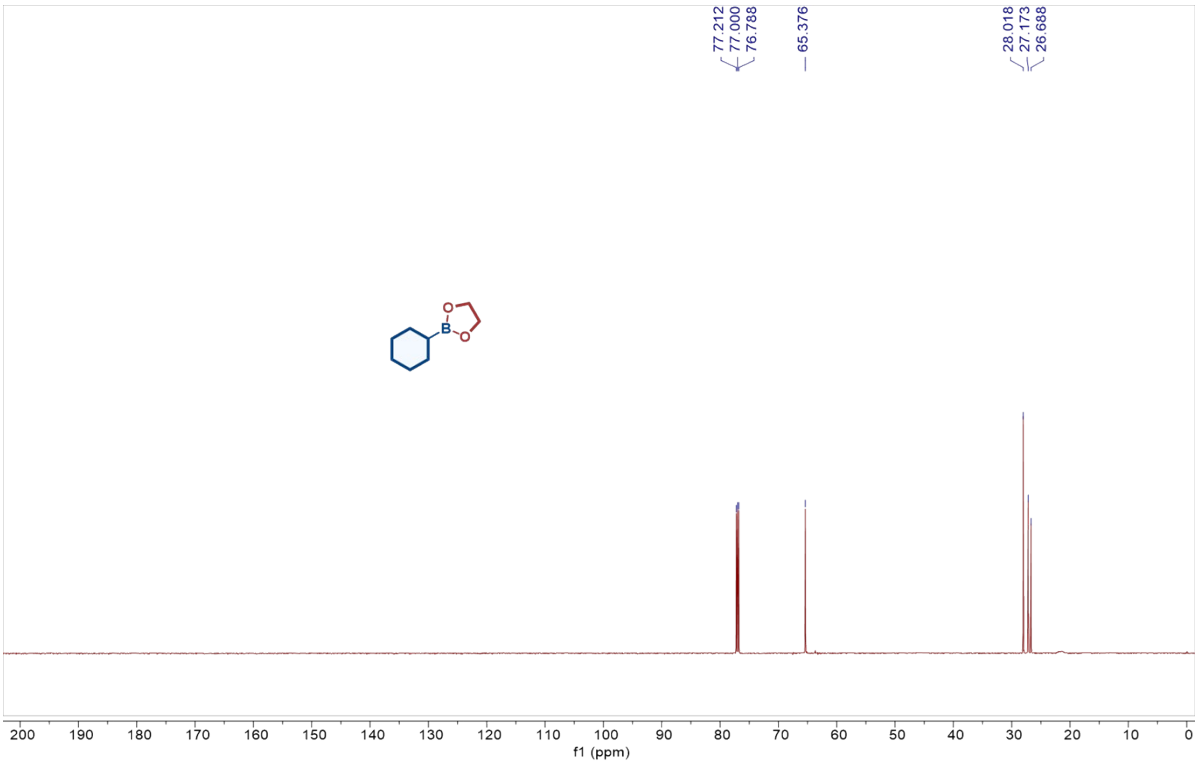

^{1}H NMR of **3w** (600 MHz, $CDCl_3$) and ^{13}C NMR of **3w** (151 MHz, $CDCl_3$)

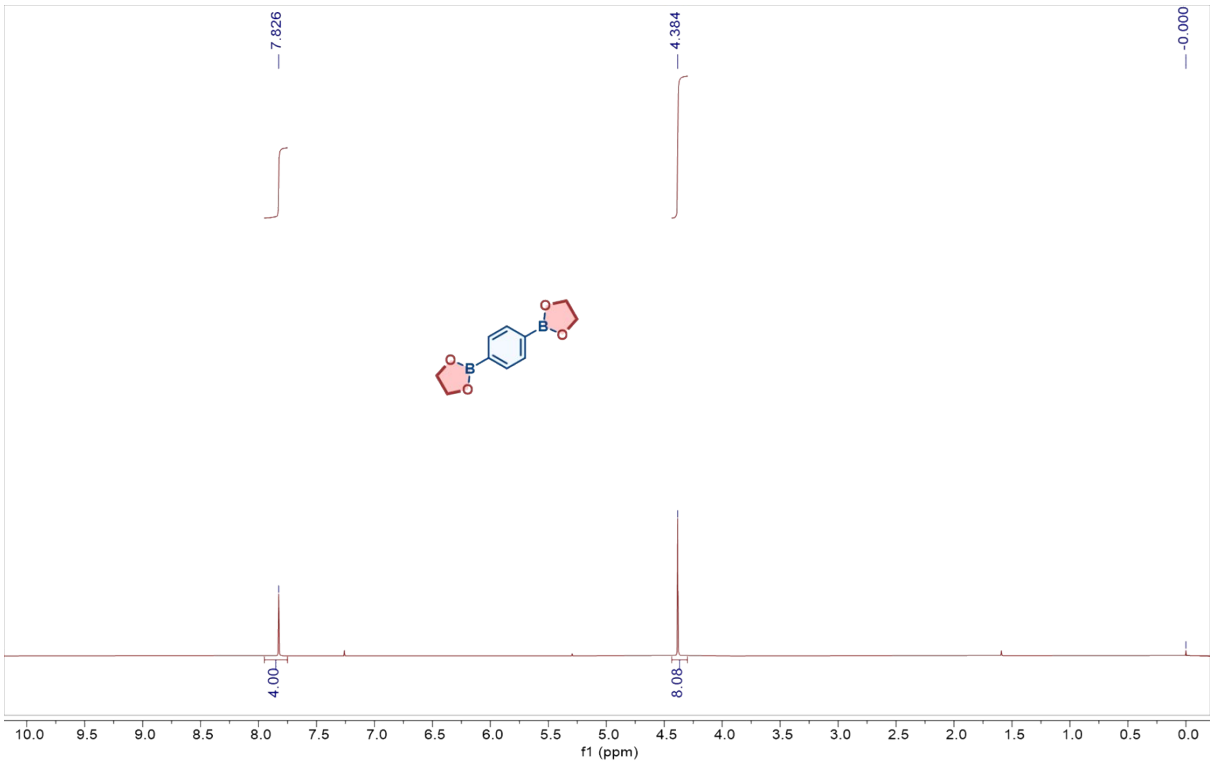

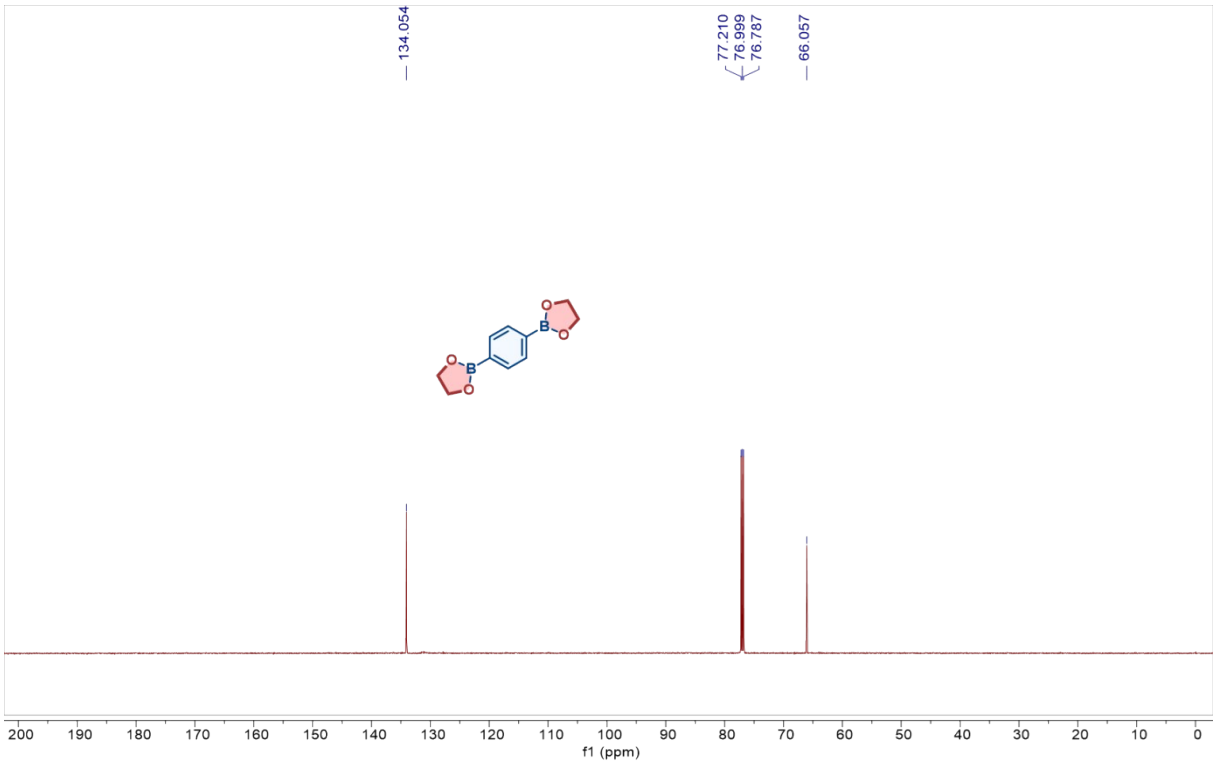

^{1}H NMR of **3x** (600 MHz, $CDCl_3$) and ^{13}C NMR of **3x** (151 MHz, $CDCl_3$)

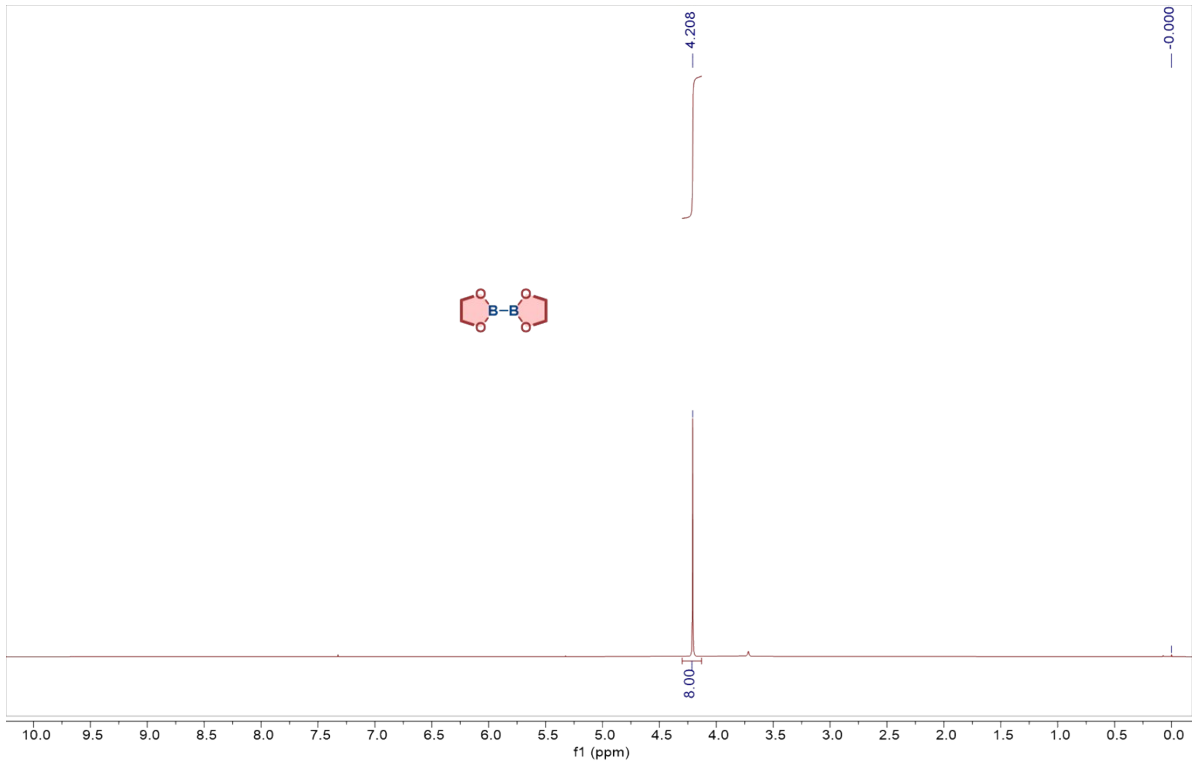

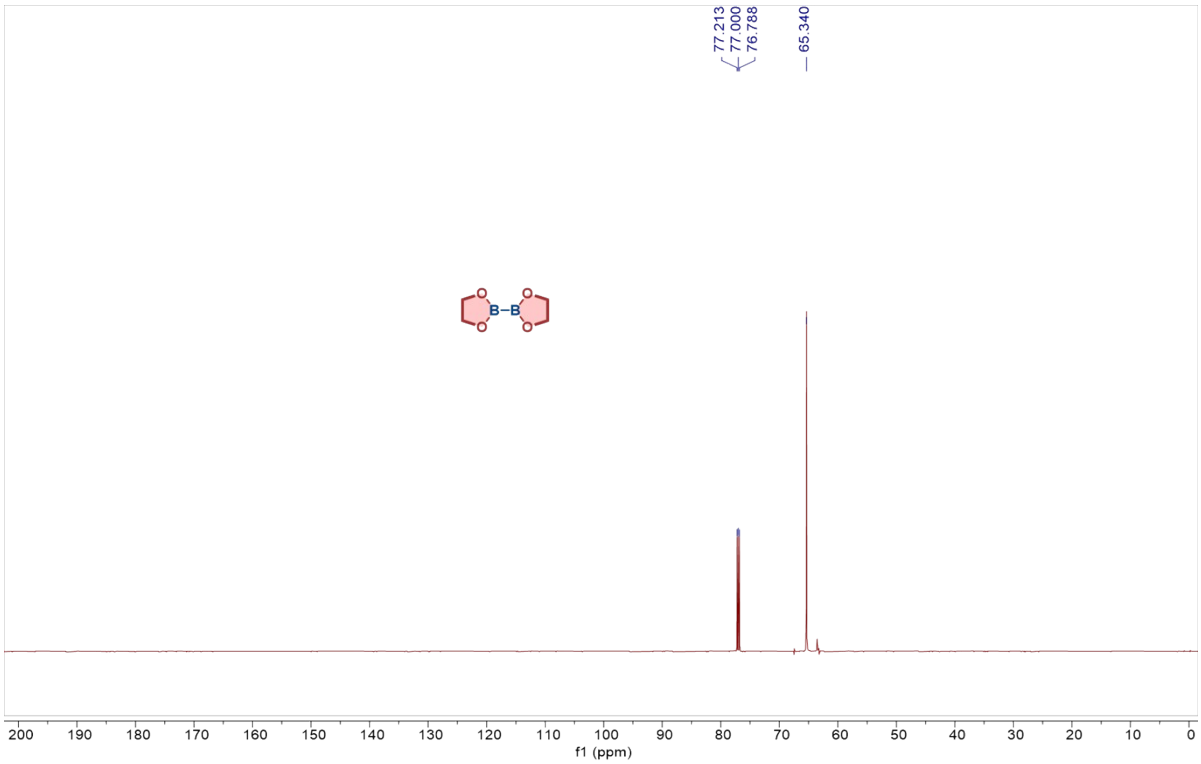

Reference

[1] Z. Q. Shen, Z. X. Jia, K. P. Yu, J. Xie, L. J. Qin, L. Gao, B. Z. Li, X. H. Wang and J. Z. Yin, *Process Saf. Environ. Protect.*, 2024, **188**, 230-238.

[2] H. Kurokawa, M. Ohshima, K. Sugiyama and H. Miura, *Polym. Degrad. Stabil.*, 2003, **79**, 529-533.

[3] S. Mishra and A. S. Goje, *Polym. Int.*, 2003, **52**, 337-342.

[4] J. T. Du, Q. Sun, X. F. Zeng, D. Wang, J. X. Wang and J. F. Chen, *Chem. Eng. Sci.*, 2020, **220**, 115642.

[5] D. D. Pham and J. Cho, *Green Chem.*, 2021, **23**, 511-525.

[6] Z. T. Laldinpuii, C. Lalmuanpuia, S. Lalhmangaihzuala, V. Khiangte, Z. Pachuau and K. Vanlaldinpuia, *New J. Chem.*, 2021, **45**, 19542-19552.

[7] S. Lalhmangaihzuala, Z. T. Laldinpuii, V. Khiangte, G. Lallawmzuali and K. Vanlaldinpuia, *Adv. Powder Technol.*, 2023, **34**, 12.

[8] S. Tanaka, J. Sato and Y. Nakajima, *Green Chem.*, 2021, **23**, 9412-9416.

[9] Z. T. Laldinpuii, V. Khiangte, S. Lalhmangaihzuala, C. Lalmuanpuia, Z. Pachuau, C. Lalhriatpuia and K. Vanlaldinpuia, *J. Polym. Environ.*, 2022, **30**, 1600-1614.

[10] B. Y. Ye, R. R. Zhou, Z. X. Zhong, S. L. Wang, H. Wang and Z. Y. Hou, *Green Chem.*, 2023, **25**, 7243-7252.

[11] S. X. Tang, F. Li, J. D. Liu, B. Guo, Z. N. Tian and J. H. Lv, *J. Chem. Technol. Biotechnol.*, 2022, **97**, 1305-1314.

[12] S. X. Tang, F. Li, J. D. Liu, B. Guo, Z. A. Tian and J. H. Lv, *J. Environ. Chem. Eng.*, 2022, **10**, 107927.

[13] J. Tang, X. S. Meng, X. J. Cheng, Q. Q. Zhu, D. X. Yan, Y. J. Zhang, X. M. Lu, C. Y. Shi and X. M. Liu, *Ind. Eng. Chem. Res.*, 2023, **62**, 4917-4927.

[14] M. S. Liu, J. Guo, Y. Q. Gu, J. Gao and F. S. Liu, *ACS Sustain. Chem. Eng.*, 2018, **6**, 15127-15134.

[15] Z. Q. Jiang, D. X. Yan, J. Y. Xin, F. Li, M. Q. Guo, Q. Zhou, J. L. Xu, Y. F. Hu and X. M. Lu, *Polym. Degrad. Stabil.*, 2022, **199**, 109905.

[16] M. Y. Ma, S. Wang, Y. Liu, H. L. Yu, S. T. Yu, C. C. Ji, H. Y. Li, G. K. Nie and S. W. Liu, *J. Appl. Polym. Sci.*, 2022, **139**, 12.

[17] J. B. Li, D. X. Yan, X. J. Cheng, C. R. Rong, J. Feng, X. Feng, J. Y. Xin, Q. Zhou, Y. Li, J. L. Xu and X. M. Lu, *Ind. Eng. Chem. Res.*, 2024, **63**, 12373-12384.

[18] X. L. Qu, G. Y. Zhou, R. Wang, B. L. Yuan, M. Jiang and J. Tang, *Green Chem.*, 2021, **23**, 1871-1882.

[19] Y. C. Liu, X. Q. Yao, H. Y. Yao, Q. Zhou, J. Y. Xin, X. M. Lu and S. J. Zhang, *Green Chem.*, 2020, **22**, 3122-3131.

[20] S. X. Chen, R. X. Liu, Y. J. Li, R. R. Zhang, C. Zhao, H. G. Tang, C. Z. Qiao and S. J. Zhang, *Catal. Commun.*, 2017, **96**, 69-73.

[21] X. X. Yu, M. M. Wang and X. R. Huang, *J. Mol. Liq.*, 2016, **216**, 354-359.

[22] P. A. Hunt, C. R. Ashworth and R. P. Matthews, *Chem. Soc. Rev.*, 2015, **44**, 1257-1288.

[23] H. L. D. Hayes, R. Wei, M. Assante, K. J. Geogheghan, N. Jin, S. Tomasi, G. Noonan, A. G. Leach and G. C. Lloyd-Jones, *J. Am. Chem. Soc.*, 2021, **143**, 14814-14826.

[24] P. A. Cox, M. Reid, A. G. Leach, A. D. Campbell, E. J. King and G. C. Lloyd-Jones, *J. Am. Chem. Soc.*, 2017, **139**, 13156-13165.

[25] M. Zhang, Y. Yu, B. Yan, X. Song, Y. Liu, Y. Feng, W. Wu, B. Chen, B. Han and Q. Mei, *Appl. Catal. B Environ. Energy*, 2024, **352**, 124055.

[26] Y. Iwai, K. M. Gligorich and M. S. Sigman, *Angew. Chem. Int. Ed.*, 2008, **47**, 3219-3222.

[27] B. Chattopadhyay, J. E. Dannatt, I. L. Andujar-De Sanctis, K. A. Gore, R. E. Maleczka, D. A. Singleton and M. R. Smith, *J. Am. Chem. Soc.*, 2017, **139**, 7864-7871.

[28] J. Y. Yu, R. Shimizu and R. Kuwano, *Angew. Chem. Int. Ed.*, 2010, **49**, 6396-6399.

[29] G. Ranjani and R. Nagarajan, *Org. Lett.*, 2017, **19**, 3974-3977.

[30] C. S. Bello and J. Schmidt-Leithoff, *Tetrahedron Lett.*, 2012, **53**, 6230-6235.

[31] C. Longstaff and M. E. Rose, *Org. Mass Spectrom.*, 1982, **17**, 508-518.

[32] M. Regueiro-Figueroa, K. Djanashvili, D. Esteban-Gómez, T. Chauvin, É. Tóth, A. de Blas, T. Rodríguez-Blas and C. Platas-Igleslas, *Inorg. Chem.*, 2010, **49**, 4212-4223.

[33] S. J. Baker, Y. K. Zhang, T. Akama, A. Lau, H. Zhou, V. Hernandez, W. M. Mao, M. R. K. Alley, V. Sanders and J. J. Plattner, *J. Med. Chem.*, 2006, **49**, 4447-4450.

[34] C. Burstein, C. W. Lehmann and F. Glorius, *Tetrahedron*, 2005, **61**, 6207-6217.

[35] G. Li, Y. Kanda, S. Y. Hong and A. T. Radosevich, *J. Am. Chem. Soc.*, 2022, **144**, 8242-8248.

[36] K. T. Wong, Y. Y. Chien, Y. L. Liao, C. C. Lin, M. Y. Chou and M. K. Leung, *J. Org. Chem.*, 2002, **67**, 1041-1044.

[37] V. Fasano, A. W. McFord, C. P. Butts, B. S. L. Collins, N. Fey, R. W. Alder and V. K. Aggarwal, *Angew. Chem. Int. Ed.*, 2020, **59**, 22403-22407.